Scuola Internazionale Superiore di Studi Avanzati - Trieste

Anion and cation permeabilities of the mouse TMEM16F/ANO6 calcium-activated channel

Thesis submitted for the degree of “Doctor Philosophiae”

Academic Year 2017/2018

Candidate:

Stefano Stabilini

Supervisors:

Prof. Anna Menini

Dott. Simone Pifferi

SISSA - Via Bonomea 265 - 34136 TRIESTE - ITALY

Abstract

TMEM16F/ANO6 is widely expressed in different tissues where it plays important physiological roles, such as the regulation of blood coagulation, bone mineralization and apoptosis. TMEM16F plays two different biological roles in cells: it acts both as scramblase and as ion channel. Both of these functions are activated by the increase of intracellular Ca^{2+} concentration.

In physiological conditions the distribution of cellular membrane lipids is polarized, meaning that the composition of the outer leaflet is different than that of the inner one. When the intracellular Ca^{2+} increases, the scramblases are activated. Scramblases are integral membrane proteins responsible for the translocation of phospholipids between the two leaflets of a lipid bilayer upon their electrochemical gradient, abolishing the asymmetry of the bilayer. This is a key process in many physiological and pathological contests because the exposure of particular lipids at the cell surface induces several transduction signalling cascades. Many studies investigated in details the molecular mechanisms of TMEM16F lipid scrambling and identified a specific domain of the protein which is essential for the lipid transport.

The mechanisms of TMEM16F ion channel activity are less clear and, in addition, several studies reported conflicting results about the ionic selectivity of the TMEM16F-mediated current. These data were partially obtained using different methodologies and analysis making difficult to reconcile the discrepancies. In particular, studies reporting that TMEM16F is more permeable for anions were performed only using the whole-cell recordings, a technique that does not allow a direct comparison of the results with or without intracellular calcium. In contrast, results showing a higher permeability for cations derive from recordings from excised patches in the inside-out configuration.

Here, we decided to investigate the ionic selectivity of TMEM16F using both configurations of the patch clamp technique, whole-cell and inside-out excised patch, using the same solutions, in order to directly compare the results. Moreover, we

investigated the properties of the Q559K mutant that has been reported to alter the ionic selectivity of TMEM16F in inside-out patches.

First of all, our study revealed a characteristic which is shared between the configurations. Indeed, TMEM16F heterologous expression in HEK 293T cells generates a large outward rectifying Ca^{2+}-activated current both in whole-cell and inside-out configuration which is due to the voltage-dependent gating of the channel. On the other hand, we found consistent differences in terms of channel time-dependent activation and selectivity. In fact, although in inside-out experiments the Ca^{2+}-dependent activation is fast and the TMEM16F-mediated current is activated in few ms, in whole-cell recordings a full activation requires up to 4 minutes. Similar results are obtained also with Q559K mutant.

In inside-out patches the Ca^{2+} concentration for half-maximal current activation ($K_{1/2}$) is 42 µM at +60 mV, while the Hill coefficient is >2. Q559K mutant shows a significant reduction of Ca^{2+} sensitivity with a $K_{1/2}$ almost 5-folds higher and a reduction of Hill coefficient to 1.4, indicating a possible alteration of the gating mechanism.

To determine the channel selectivity, we decided to calculate the relative permeability between Na^+ and Cl^- (P_{Na}/P_{Cl}) using the dilution method both in whole-cell and inside-out configuration. We found that TMEM16F-mediated current is highly non-selective but there are differences depending on the configuration of the recordings. Indeed, in whole-cell both TMEM16F wild type and Q559K mutant have a P_{Na}/P_{Cl} around 0.5 indicating a slight preference for Cl^- permeation. In contrast, in inside-out experiments the Q559K mutant retains a higher permeability for Cl^-, while TMEM16F wild type channel shows a higher permeability for Na^+ with a P_{Na}/P_{Cl} reaching 3.6.

These results have two major implications: First, the discrepancies found between the recordings in whole-cell and inside-out, could suggest the presence of a cellular mechanism factor which controls TMEM16F selectivity. When the patch is excised this cellular mechanism and its controlling activity are lost. Second, the residue in position 559 could be responsible to control the selectivity among cations and anions when this cellular mechanism is lost.

Table of Contents

1. Introduction ---- 1

1.1. TMEM16 family ---- 1

1.1.1. Identification and classification ---- 1

1.1.2. Physiological functions of TMEM16A ---- 3

1.1.3. Physiological functions of TMEM16B ---- 5

1.1.4. TMEM16A and TMEM16B biophysical properties ---- 5

1.1.4.1. Activation by Ca^2 ---- 5

1.1.4.2. Anion selectivity ---- 8

1.1.5. Structure ---- 8

1.2. TMEM16F ---- 10

1.2.1. Pattern of expression and physiological functions ---- 10

1.2.2. Biophysical properties ---- 12

1.2.2.1. Activation by Ca^{2+} ---- 12

1.2.2.2. Rundown and modulation by PIP_2 ---- 13

1.2.2.3. Ion selectivity ---- 15

1.2.3. Scramblase activity ---- 17

1.2.3.1. Membrane asymmetry and lipid transporters ---- 17

1.2.3.2. Identification of TMEM16F scramblase activity ---- 18

1.2.3.3. Structure and possible mechanisms of scrambling ---- 19

1.2.3.4. Relationship between scramblase and channel activities ---- 22

2. Project aim ---- 24

3. Materials and Methods ---- 25

3.1. Cell culture and transfection ---- 25

3.2. Electrophysiological recording ---- 25

3.3. The perfusion system ---- 26

3.4. Solutions ---- 27

3.5. Data analysis ---- 28

4. Results ---- 29

5. Discussion ---- 53

6. References ---- 56

1. Introduction

1.1. TMEM16 family

1.1.1. Identification and classification

In 2008 three laboratories reported independently that TMEM16A encoded for Calcium Activated Chloride Channels (CaCCs) (Caputo et al., 2008; Schroeder et al., 2008; Yang et al., 2008). Lately, in 2009, other papers extended the characterization of TMEM16B as CaCC (Pifferi et al., 2009; Stephan et al., 2009; Stöhr et al., 2009). Surprisingly, in 2010 Suzuki et al. reported that TMEM16F encoded for a Ca^{2+}-dependent scramblase. Further investigation indicated that also TMEM16C, D, E, F, G, H and J are able to mediate lipid scrambling (Di Zanni et al., 2018; Gyobu et al., 2017; Suzuki et al., 2013). However, TMEM16F and E seem also to mediate Ca^{2+}-dependent ion currents, while TMEM16C modulates the activity of the Na^{+}-activated K^{+} channel SLACK (Falzone et al., 2018).

The TMEM16 gene family is present in the genome of all the eukaryotic organisms from fungi to animals (Milenkovic et al., 2010). In the Chordata phylum, the TMEM16 family consists of 10 members, named with the letters from A to K (excluding I). An alternative name for TMEM16 proteins is “Anoctamin” (shorted as “Ano”) numbered from 1 to 10 (Figure 1). The name “Anoctamin” was initially proposed because the first characterized TMEM16 family member, TMEM16A, is anion selective and bioinformatic hydropathy analysis predicted that TMEM16A have eight transmembrane domains. However, more recent findings show that TMEM16 proteins are composed of 10 transmembrane domains and not all are channel selective for anions. For these reasons, we prefer to use the more general name “TMEM16”.

The comparison of the TMEM16 family members sequences suggested that these proteins can be evolutionary related and share a common ancestor (Hahn et al., 2009; Milenkovic et al., 2010).

The TMEM16 proteins are differently expressed in different tissues. TMEM16B, C and D are mostly expressed in neuronal tissues. In particular, photoreceptor and chemosensory neurons of the nasal cavity, such as olfactory and vomeronasal sensory neurons, highly express TMEM16B (Dauner et al., 2012; Dibattista et al., 2012, 2012; Maurya and Menini, 2014; Stephan et al., 2009; Stöhr et al., 2009). Moreover, TMEM16B has been found in thalamocortical, inferior olivary and hippocampal neurons (Ha et al., 2016; Huang et al., 2012; Zhang et al., 2017). Conversely, TMEM16C and D have a similar expression in the spinal cord, brain stem, cerebellum and eye. TMEM16C is also

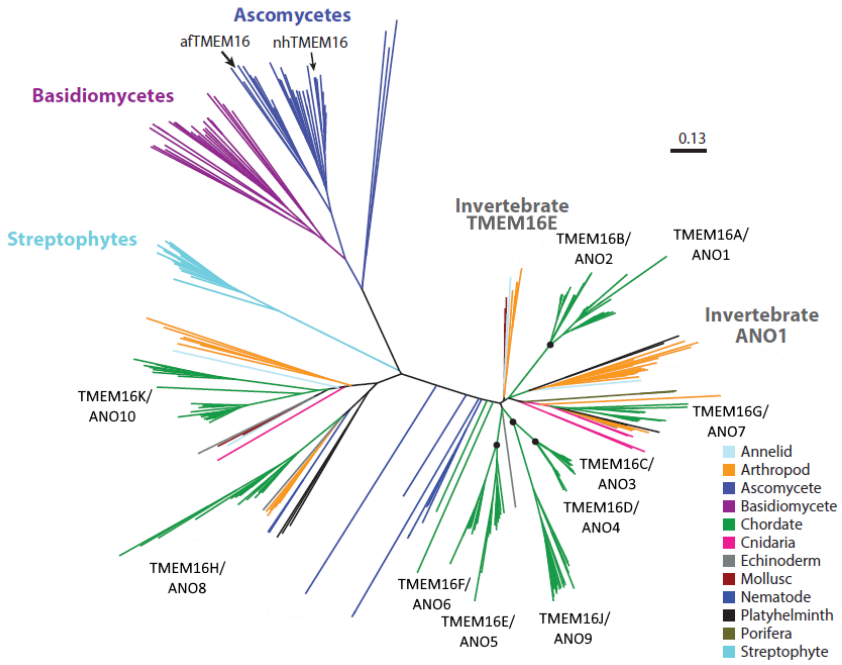

Figure 1. *Schematic representation of TMEM16 family members in eukaryotic organisms with branches colored according to phylum. Chordate ANOs 1–10 are colored in green. Other phyla are colored according to the key. (Modified from Withlock & Hartzell, 2017).*

expressed in rat dorsal root ganglion neurons (Huang et al., 2013). TMEM16F, H and K, are almost ubiquitously expressed, even if with different levels of expression (Schreiber et al., 2010). TMEM16A, E, G, and J are mainly localized in the epithelia tissues (Schreiber et al., 2010). In particular, supporting cells of the olfactory epithelium and vomeronasal sensory neurons express TMEM16A (Amjad et al., 2015; Dauner et al., 2012; Dibattista et al., 2012; Maurya and Menini, 2014).

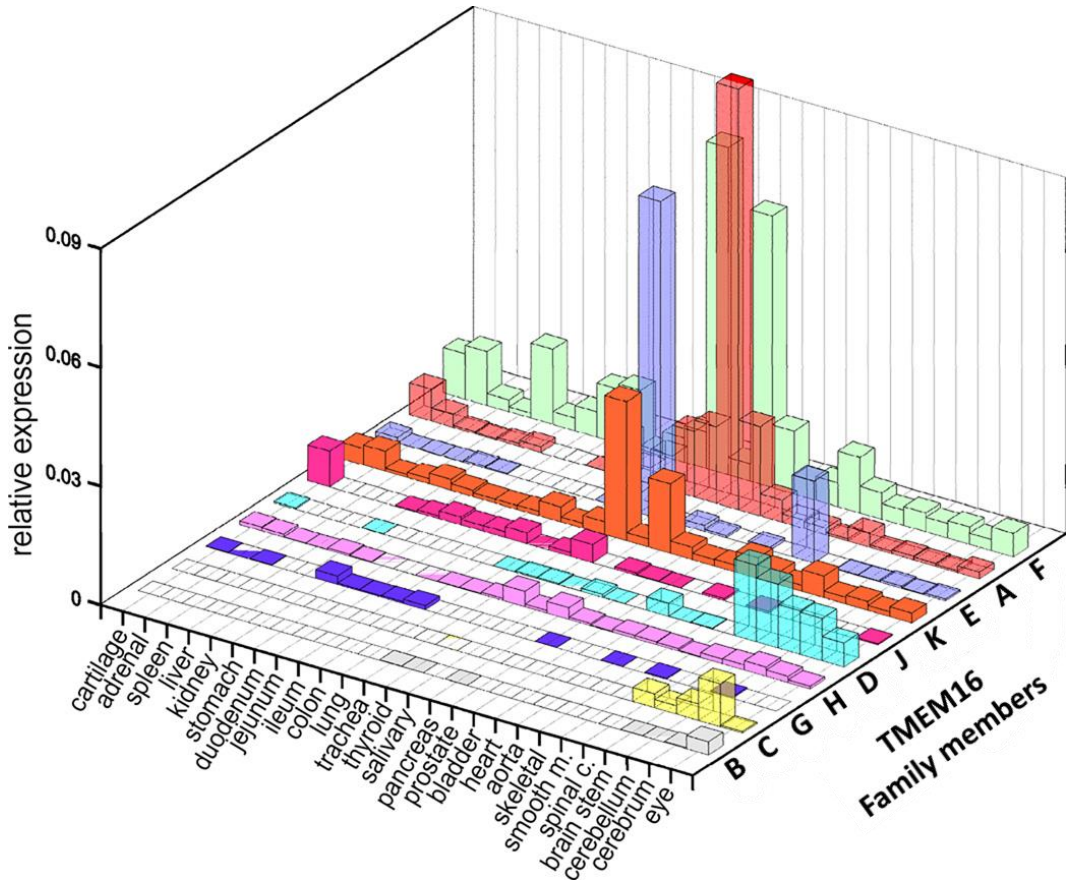

Figure 2. *Expression of TMEM16 members mRNA in murine tissues obtained by Real-time RT-PCR. Expression of mRNA for ANO1–10 was normalized using expression of β-actin as a reference (Modified from Screiber et al., 2010)*

1.1.2. Physiological functions of TMEM16A

Several studies showed that TMEM16A plays important roles in controlling secretion in different epithelial tissues. For example, the cytokine interleukin-4 (IL-4) and interleukin-13 (IL-13) activate the secretion of the human bronchial epithelial cells inducing a Ca^{2+} dependent Cl^- conductance in the apical membrane (Danahay et al., 2002; Galietta et al., 2002). In the same system, Caputo et al. (2008) found that IL-4 induces the overexpression of TMEM16A and the knock-down of TMEM16A impairs the secretion activated by IL-4.

Similar results were also obtained in the kidney. Indeed, TMEM16A is expressed in the Madin-Darby canine kidney (MDCK) cells that resemble the principal cells of the

collecting duct and pharmacological inhibition of TMEM16A or silencing using RNAi caused a reduction of purinergic-induced secretion (Buchholz et al., 2014). Moreover, in different models of kidney cysts, TMEM16A knock-down inhibited the cyst's growth and enlargement, opening the possibility to use TMEM16A as a new therapeutic target for polycystic kidney disease (Buchholz et al., 2014).

TMEM16A is expressed in smooth muscle cells of arteries and veins (Davis et al., 2010, 2013; Manoury et al., 2010; Thomas-Gatewood et al., 2011) and seems to be involved in the myogenic response in cerebral arteries. Indeed, knock-down of TMEM16A abolishes the vasoconstriction of cerebral arteries and depolarization of vascular smooth muscle cells (Bulley et al., 2012). Indeed, TMEM16A has been found upregulated in several pulmonary hypertension models (Forrest et al., 2012; Sun et al., 2012).

Upregulation of TMEM16A has been observed in many cancer types, such as lung cancer (Jia et al., 2015), breast cancer (Britschgi et al., 2013; Wu et al., 2015), glioma (Liu et al., 2014), prostate cancer (Liu et al., 2012) and many others (Bill et al., 2015; Dixit et al., 2015; Sauter et al., 2015; Sui et al., 2014). TMEM16A seems to be highly associated with tumor and its progression. Indeed, TMEM16A overexpression shows a relevant correlation with:

- Low survival in patients affected by cancer (Britschgi et al., 2013; Duvvuri et al., 2012; Ruiz et al., 2012).
- Enhanced cell migration (Ayoub et al., 2010).
- Increased tumor growth and metastasis (Liu et al., 2012).

In addition, TMEM16A is expressed in dorsal root ganglia (DRG) nociceptive neurons (Yang et al., 2008). Importantly, TMEM16A knock-down decreases the amplitude of CaCC currents in DRG nociceptors activated by the inflammatory mediator bradykinin (Liu et al., 2010). Moreover, Cho et al. (2012) found that TMEM16A is highly responsive to heat. Indeed, temperatures higher than 44°C activate TMEM16A currents also in the absence of intracellular Ca^{2+}. Conditional knock-out of TMEM16A in DRG neurons causes a decrease in the heat sensitive current and greatly reduces the nociceptive behavior in thermal pain models (Cho et al., 2012).

1.1.3. Physiological functions of TMEM16B

The physiological role of TMEM16B has been intensively investigated in the olfactory sensory neurons (OSNs). Indeed, TMEM16B is highly expressed in the cilia of the OSNs (Dauner et al., 2012; Dibattista et al., 2012; Rasche et al., 2010; Stephan et al., 2009), in which it is involved in controlling the duration of firing and axonal targeting in response to a stimulus (Pietra et al., 2016). Using a knock-out mice model, Billig et al. (2011) showed that TMEM16B mediated the Ca^{2+}-activated Cl^- current involved in the olfactory transduction. However, they reported that these mice did not show defects in olfactory-driven behaviors (Billig et al., 2011). These results were partially challenged by more recent studies showing that the lack of TMEM16B caused an impairment in different olfactory-driven behaviors that did not require training or learning (Dibattista et al., 2017; Neureither et al., 2017; Pietra et al., 2016).

TMEM16B is also present in the presynaptic terminal of the mouse photoreceptors. Stöhr et al. (2009) showed that TMEM16B forms a complex with the presynaptic proteins PSD95, VELI3 and MPP4 and, remarkably, the lack of MPP4 abolishes also the expression of TMEM16B (Stöhr et al., 2009).

TMEM16B controls action potential firing in several neuronal cell types such as hippocampal, thalamocortical and inferior olivary neurons (Ha et al., 2016; Huang et al., 2012; Zhang et al., 2017).

1.1.4. TMEM16A and TMEM16B biophysical properties

1.1.4.1. Activation by Ca^2

TMEM16A and TMEM16B are CaCCs (Caputo et al., 2008; Pifferi et al., 2009; Schroeder et al., 2008; Stephan et al., 2009; Stöhr et al., 2009; Yang et al., 2008), activated by a cytosolic increase of Ca^{2+} concentration. In both channels, the Ca^{2+} activation is influenced by voltage. Specifically, when TMEM16A was expressed in HEK-293 cells the EC_{50} for Ca^{2+} was 2.6 μM at -60 mV and 0.4 μM at +60 mV, revealing a remarkable voltage dependence (Figure 3a; (Yang et al., 2008)). In addition, Ferrera et

al. (2009) showed that different TMEM16A splicing variants exhibit diverse Ca^{2+} sensitivity. TMEM16B is less sensitive to Ca^{2+} than TMEM16A even if there are differences between the various splice variants. Indeed, Pifferi et al. (2009) reported values for EC_{50} for Ca^{2+} of 4.9 µM at -50 mV and 3.3 µM at +50 mV for retinal isoform (Figure 3b), and Stephan et al. (2009) found EC_{50} values of 1.83 µM at -40 mV and 1.18 µM at +40 mV for olfactory isoform (Pifferi et al., 2009; Stephan et al., 2009). Similar to TMEM16A, also TMEM16B has splicing variants with different Ca^{2+} sensitivities (Ponissery Saidu et al., 2013).

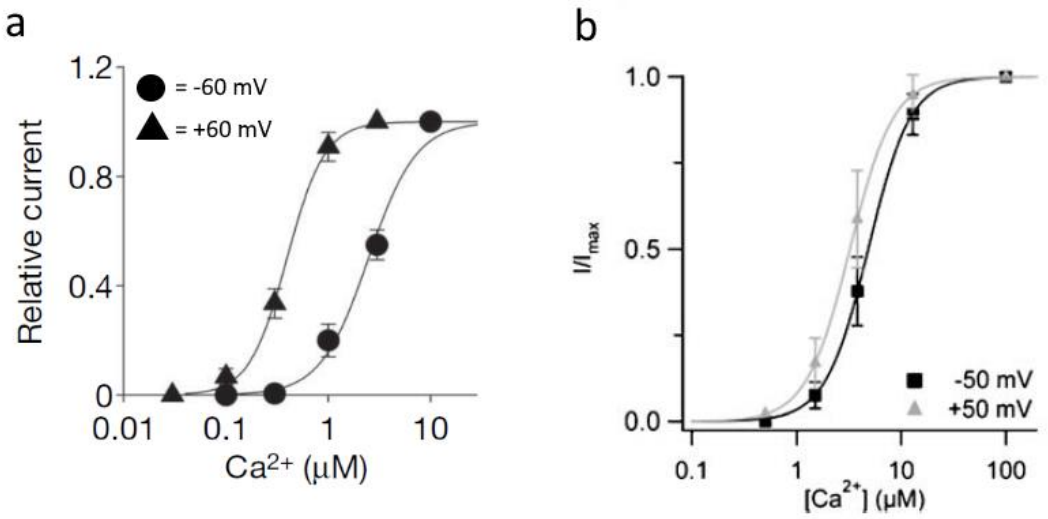

***Figure 3**. **(a)** Dose–response relationships of TMEM16A-mediated currents in HEK cells in inside-out experiments. Current responses were normalized to the value in the presence of 100 µM Ca^{2+}. The Hill coefficient was 2.0 at -60 mV and 2.4 at +60 mV. EC_{50} was 2.6 µM Ca^{2+} at −60 mV, and 0.3 µM Ca^{2+} at +60 mV (Modified from Yang et al., 2008). **(b)** Dose–response relationships of retinal TMEM16B-mediated currents in HEK cells in inside-out experiments. Current responses were normalized to the value in the presence of 100 µM Ca^{2+}. The Hill coefficient was 2.5 at −50 mV and 2.0 at +50 mV. EC_{50} was 4.9 µM Ca^{2+} at −50 mV, and 3.3 µM Ca^{2+} at +50 mV (Pifferi et al., 2009).*

Another shared feature between TMEM16A and TMEM16B is an irreversible current rundown. The rundown is a progressive and unrestrainable decrease of the current amplitude, upon Ca^{2+} application, when the channels are recorded in excised patches (Chen et al., 2011; De Jesús-Pérez et al., 2018; Ni et al., 2014; Pifferi et al., 2009). In order to determine the rundown mechanism, Pifferi et al. (2009) added several molecules to the cytoplasmic side of the excised patches (Na_3VO_4, DTT, Calmodulin, cAMP, PIP_3), but none of them reduced the rundown (Pifferi et al., 2009). More recently,

De Jesús-Pérez et al. (2018), showed that Phosphatidylinositol (4,5)-bisphosphate (PIP_2) can decelerate TMEM16A rundown and partially recover the current decrease (De Jesús-Pérez et al., 2018).

In spite of the extensive efforts, the role of Calmodulin (CaM) in TMEM16A/B regulation is still not completely clear. Tian et al. (2011) reported that the activation of the TMEM16A channel by intracellular Ca^{2+} required CaM (Tian et al., 2011). However, Terashima et al. (2013) showed that purified TMEM16A reconstituted in artificial liposomes is sufficient to recapitulate the biophysical properties of TMEM16A measured with patch-clamp experiments. They also showed investigated if TMEM16A and Ca^{2+}-CaM could be formed complex in vitro. Using size-excluding chromatography and pull down experiments, they did not detect interaction between TMEM16A and Calmodulin. (Terashima et al., 2013).This result have been lately confirmed by another group using a co-immunoprecipitation assay (Yu et al., 2014).

More recently, Yang and Colecraft (2016), using a bioengineering approach named ChIMP (Channel Inactivation induced by Membrane-tethering of an associated Protein), found that Ca^{2+}-free CaM (apoCaM) is pre-associated with both TMEM16A and 16B channels. They suggested that this pre-association mediates different effects depending on the Ca^{2+} concentration. At a low level of intracellular Ca^{2+}, calmodulin induces a Ca^{2+}-dependent sensitization increasing the Ca^{2+} sensitivity. Whereas, at high intracellular Ca^{2+} concentration, calmodulin is responsible for a Ca^{2+}-dependent inactivation. This modulation depends on the splice variant and it is lost in TMEM16A lacking the exon *b* (Yang and Colecraft, 2016).

However, we are still missing a complete understanding of molecular details of the calmodulin binding sites and whether calmodulin regulates TMEM16A in vivo.

Interestingly, it has been observed that Ca^{2+}-dependent current activation, deactivation kinetics and Ca^{2+}-sensitivity of both TMEM16A and 16B channels are modified by different permeant anions, showing that gating of these channels is modulated by permeant anions (Betto et al., 2014; Perez-Cornejo et al., 2004; Xiao et al., 2011).

1.1.4.2. Anion selectivity

TMEM16A and TMEM16B are selective for anions with permeability ratios similar to those of native CaCCs. In particular, SCN^-, I^-, NO_3^- and Br^- are more permeant than Cl^-, whereas gluconate, F^- and methanesulfonate (MeS) are less permeant than Cl^- (Adomaviciene et al., 2013; Reyes et al., 2014; Sagheddu et al., 2010; Schroeder et al., 2008; Yang et al., 2008) See Figure 4).

Interestingly, TMEM16A and TMEM16B anionic selectivity is dynamic during channel activation. Indeed, it has been shown that by replacing Cl^- with more permeant anions, the Ca^{2+}-activated current revealed two different components with different permeability ratios (Sagheddu et al., 2010; Schroeder et al., 2008). These results confirmed a previous study on native channels suggesting that CaCC currents in Xenopus oocytes may have various components with different anion selectivity (Kuruma and Hartzell, 1999).

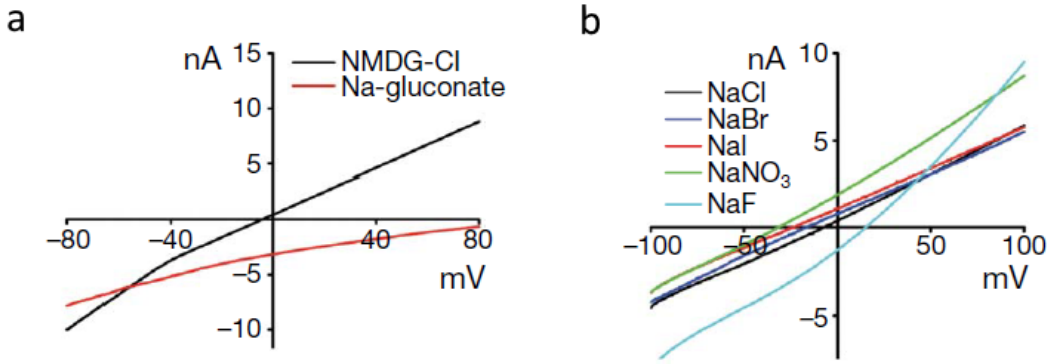

Figure 4. *Current-voltage relations of TMEM16A current, in inside-out patches, upon perfusion of different salts (Yang et al., 2008).* ***(a)*** *Bath solutions contained 140 mM NMDG-Cl or Na-gluconate.* ***(b)*** *Bath solution contained 140 mM NaCl, NaBr, NaI, $NaNO_3$ or NaF (Yang et al., 2008).*

1.1.5. Structure

Brunner et al. (2014) first described the X-ray structure of a TMEM16 family member: the nhTMEM16 from the fungus *Nectria haematococca.* They showed that the protein is a homodimer and that each subunit contains ten transmembrane domains (TDs) and a hydrophilic cavity that crosses the membrane. This cavity presents a

conserved Ca^{2+}-binding site located within the hydrophobic core of the membrane. In addition, Brunner et al. (2014) also carried out functional experiments on nhTMEM16 and TMEM16A with mutations in the putative Ca^{2+} binding site and suggested that Ca^{2+}

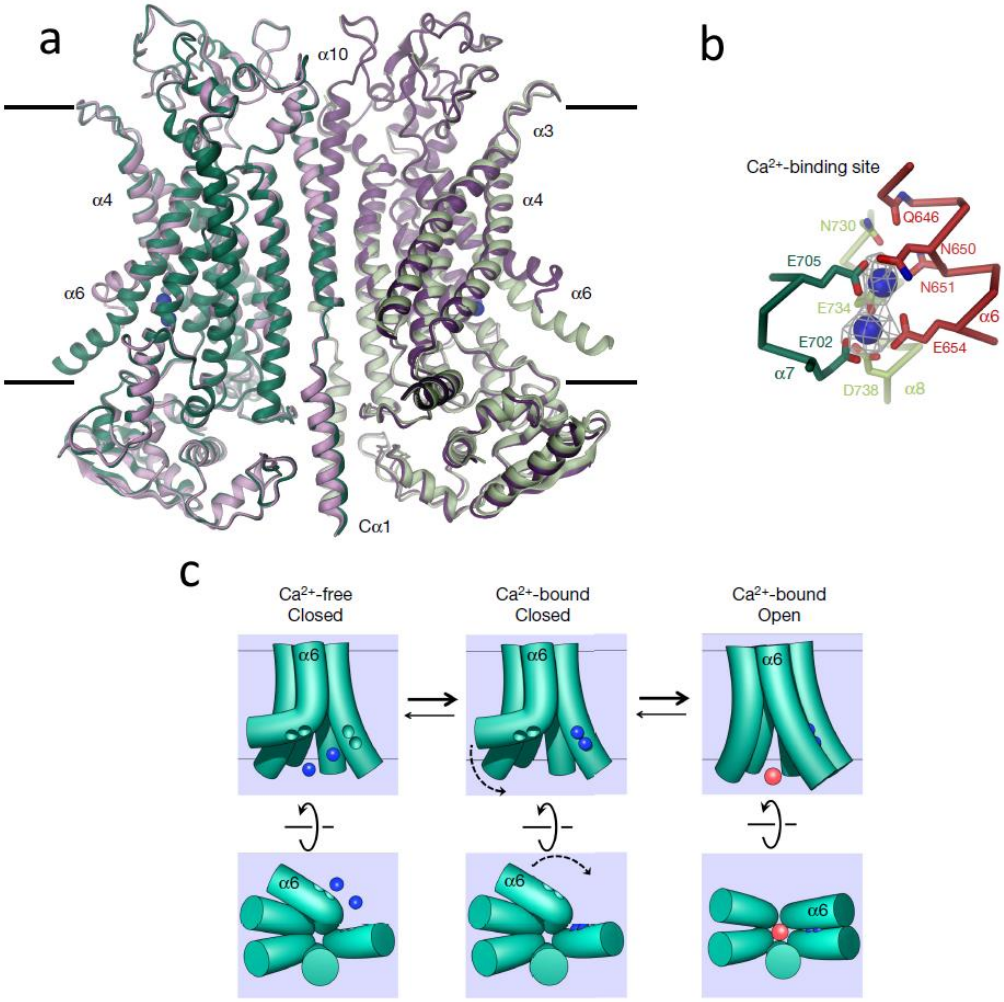

Figure 5. (a) *Ribbon representation of a superposition of the Ca^{2+}-bound (in green) and Ca^{2+}-free (in violet) structures of mTMEM16A. Black lines represent membrane leaflets and the blue spheres are Ca^{2+} ions in the Ca^{2+}-bound conformation.* ***(b)*** *Structure of Ca^{2+}-binding site, showing the residues interacting with two Ca^{2+} ions.* ***(c)*** *Schematic representation of TMEM16A activation. Top panels represent a view in the membrane, while bottom panels show a view from the intracellular side. Green cylinders are the transmembrane domains. In the absence of bound Ca^{2+} (blue sphere), TD6 is bended remaining distant from TD7. The binding of Ca^{2+} induces a conformational change in TD6, which gets close to TD7, opening the channel and allowing Cl^- (red sphere) permeation (Modified from Paulino et al.,2017).*

activation of the two proteins is regulated by equivalent residues (Brunner et al., 2014).

More recently, Paulino et al. (2017a) and Dang et al. (Dang et al., 2017) characterized the mouse TMEM16A structure using Cryogenic Electron Microscopy

(Cryo-EM). They confirmed the homodimeric structure, with subunits composed of ten TDs, and cytosolic N- and C-terminal (Figure 5a). Each subunit contains an ion conducting pore which is surrounded by TD3-TD7. The shape of the pore resembles an hourglass, with a small extracellular and a big intracellular regions, connected by a tight neck region. The same groups also identified a Ca^{2+}-binding site (Figure 5b), present in each subunit, composed of five residues localized on TD6, TD7 and TD8, confirming the previous functional TMEM16A characterization, in which these residues were described as affecting Ca^{2+} sensitivity (Tien et al., 2014; Yu et al., 2012). Interestingly, a pronounced difference between the TMEM16A's structure in the presence or absence of Ca^{2+} has been observed. In the presence of Ca^{2+}, the intracellular regions of TD6 and TD7 are in close proximity and interact with Ca^{2+} ions, activating the channel. Conversely, when Ca^{2+} is absent, the lower part of TD6 moves toward TD4, increasing the distance from TD7 (Figure 5c). This TD6 rearrangement can be described by a movement around the G644 residue that acts as a pivot. When replacing G644 with less flexible amino acids, TMEM16A Ca^{2+}-sensitivity increases and, in particular, the G644P mutation produces a constitutive channel activation even in the absence of Ca^{2+}. More recently, another study has confirmed the involvement of TD6 in TMEM16A gating (Peters et al., 2018).

1.2. TMEM16F

1.2.1. Pattern of expression and physiological functions

TMEM16F is very broadly expressed in several different tissues, such as bones, skin, lungs, muscles, kidneys, pancreas, thyroid, and blood cells (Ehlen et al., 2013; Schreiber et al., 2010; Scudieri et al., 2015; Shimizu et al., 2013). TMEM16F was firstly described as a lipid scramblase and only later as ion channel (Martins et al., 2011; Suzuki et al., 2010).

TMEM16F is involved in several physiological functions:

- *Blood coagulation*. The scrambling activity of TMEM16F exposes phosphatidylserine (PS) to the external side of the plasma membrane. On platelets, the PS exposed on platelets is a triggering signal for the coagulation

cascade (Baig et al., 2016; van Kruchten et al., 2013; Yang et al., 2012). The involvement of TMEM16F in coagulation is also confirmed by loss-of-function mutation in mice, which leads to a bleeding disorder similar to a human condition called “Scott syndrome” (Fujii et al., 2015; Yang et al., 2012).

- *Bone mineralization*. It has been demonstrated that during skeletogenesis, TMEM16F mRNA is highly present in differentiating and mature osteoblasts and TMEM16F-KO mice present reduced skeleton size and skeletal deformities (Ehlen et al., 2013). These defects could be explained by the finding that TMEM16F is required for the proper function of Na^+/Ca^{2+} exchanger NCX1, which moves Ca^{2+} out of osteoblasts into the calcifying bone matrix (Ousingsawat et al., 2015a).
- *Cell migration*. Knock-down of TMEM16F decreases the rate of the Ehrlich Lettre ascites (ELA) cells migration by 40% (Jacobsen et al., 2013).
- *Immunity*. TMEM16F is present on mast cell cellular membranes and because of its scramblase function, it appears to be involved in mast cells activation (Rysavy et al., 2014). TMEM16F is also implicated in the stimulation of the migration and bacterial phagocytosis by macrophages (Ousingsawat et al., 2015b). Moreover, TMEM16F seems to have a role also in chemokine-induced migration of dendritic cells. Indeed, when TMEM16F is ablated, the migration is reduced (Szteyn et al., 2012).
- *Apoptosis*. TMEM16F seems to be involved in extrinsic apoptotic pathways. Indeed, Fas Ligand (FasL) stimulation induces both TMEM16F current and PS exposure, subtending an involvement of TMEM16F in apoptosis (Kmit et al., 2013). Moreover, silencing of TMEM16F reduces cell death induced by staurosporine (Martins et al., 2011) and decreases caspase-3 activity induced by cisplatin (Juul et al., 2014).

1.2.2. Biophysical properties

1.2.2.1. Activation by Ca^{2+}

TMEM16F current activation is Ca^{2+}-dependent, as previously shown for TMEM16A and 16B. Yang et al. (2012) compared the Ca^{2+}-dependence of endogenous and heterologously expressed TMEM16F currents in inside-out excised patches. At +60 mV, they estimated values for EC_{50} for Ca^{2+} of 13.6 µM in HEK-293 cells and 5.1 µM in megakaryocytes and suggested that the difference might be due to a native regulator, which is lost in HEK-293 cells. Moreover, Yang et al. (2012) found that the E667Q mutant greatly reduces the Ca^{2+}-sensitivity to 2.8 mM, about 2,000 fold higher than the value of 13.6 µM measured in the wild type channel, indicating an essential role of this residue in Ca^2 binding (Yang et al., 2012). The resolution of the TMEM16A structure has indeed confirmed these results, showing that residue E667 is one of the five conserved amino acids constituting the Ca^{2+}-binding site (Paulino et al., 2017a).

Shimizu et al. (2013) and Scudieri et al. (2015), using whole-cell configuration on HEK-293 cells transfected with TMEM16F, respectively found EC_{50} values for Ca^{2+} of 9.6 µM and 11.6 µM at +100 mV (Scudieri et al., 2015; Shimizu et al., 2013). Grubb et al. (2013) found a higher EC_{50} value of 105 µM Ca^{2+} at +70 mV (Grubb et al., 2013). A low EC_{50} value of 839 nM Ca^{2+} at -80 mV has also been reported by measuring the Ca^{2+} concentration released from intracellular stores upon ATP stimulation with ratiometric calcium imaging (Henkel et al., 2015).

All the results obtained using whole-cell recordings showed that the TMEM16F current takes several minutes to activate completely and the time of activation is related with Ca^{2+} concentration (Grubb et al., 2013; Kim et al., 2015).

Recently it has been reported that the current rundown affects Ca^{2+}-sensitivity (Figure 6 a-c), changing the EC_{50} for Ca^{2+} from 7 µM to 45 µM at +80 mV (Ye et al., 2018).

This finding could partially explain the large range of Ca^{2+}-sensitivities obtained in different reports.

1.2.2.2. Rundown and modulation by PIP_2

TMEM16F current undergoes current rundown during inside-out recordings and the results are similar to those obtained for TMEM16A and 16B. Indeed, Ye et al. (2018) showed that during the application of 1 mM Ca^{2+} for 60 seconds, the current amplitude was dramatically reduced to about 50% before it reached a stable condition (Figure 6a). Moreover, current rundown decreases also TMEM16F Ca^{2+} sensitivity, from 7 µM to 45 µM, revealing channel desensitization (Figure 6b). In many ion channels current rundown is due to the reduction of phosphatidylinositol 4,5-bisphosphate (PIP_2) or phosphatidylinositol 3,4,5-bisphosphate (PIP_3) in the membrane during long excised patch recordings (Hille et al., 2015; Rohacs, 2014; Taylor and Sanders, 2017). Many data from Ye et al. (2018) found a similar scenario also for TMEM16F. Using Mg^{2+}-ATP, which maintains the activity of the kinases responsible for phosphoinositides (PI) phosphorylation, they found a partial recovery of the current amplitude, suggesting that PIP_2 has a role in TMEM16F modulation (Figure 6c). Furthermore, application of Poly-L-lysine (PLL), a known PIP_2 scavenger, the current amplitude and Ca^{2+} sensitivity (Figure 6d and 6e).

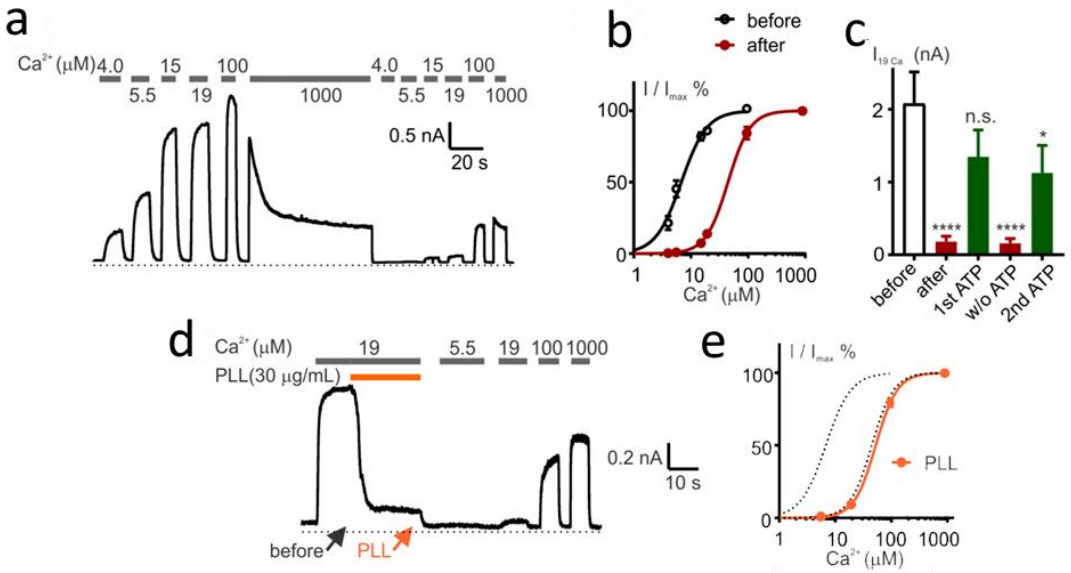

Figure 6. (a) *Inside-out patch recordings from a TMEM16F transfected cell exposed to different [Ca^{2+}], showing current rundown.* ***(b)*** *Ca^{2+} sensitivity before (black) and after (red) current rundown.* ***(c)*** *Histogram reporting the effect of ATP perfusion.* ***(d)*** *PLL effect of current amplitude.* ***(e)*** *Ca^{2+} sensitivity after PLL treatment (modified from Ye et al., 2018).*

The addition of synthetic dipalmitoyl-PIP_2 (di-C16 PIP_2) and natural PIP_2 isolated from swine brain produced a partial recover of current amplitude, and remarkably, PIP_2-induced recovery was maintained also after its removal from the solution, indicating that it was incorporated in the patch membrane (Figure 7a, b). By testing different PI derivatives, Ye et al. (2018) found that the interaction between TMEM16F and PI derivatives had low specificity, but two phosphate groups were required to recover the current (Figure 7c).

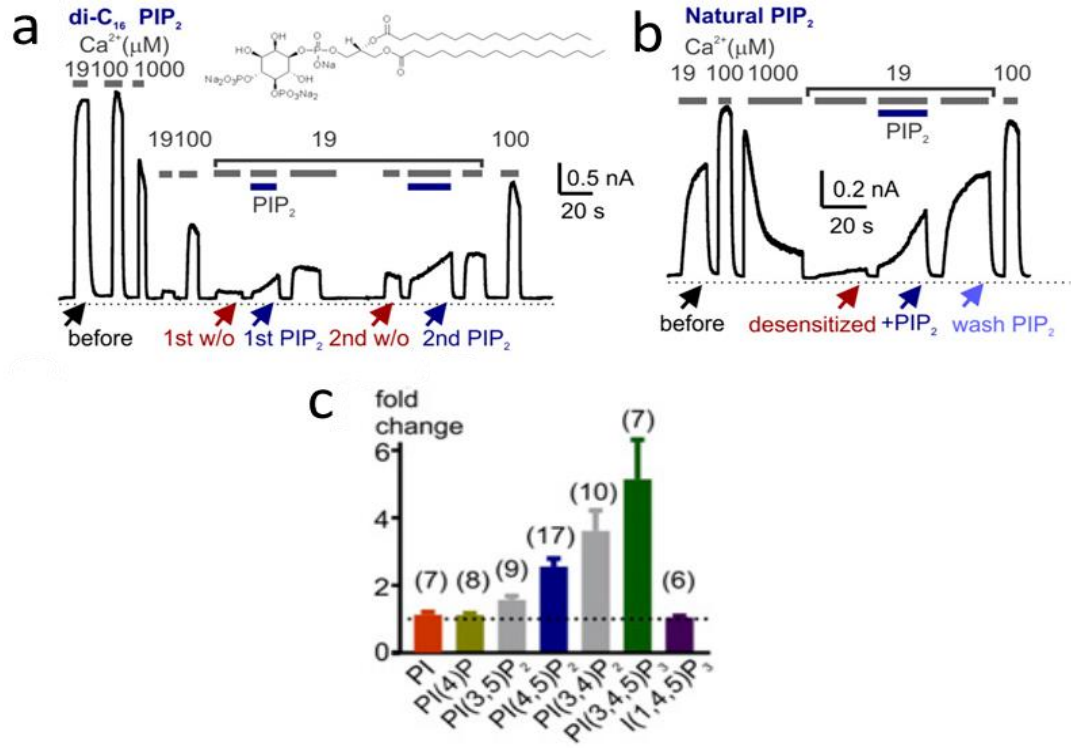

Figure 7. (a,b) *Recovery of current induced by di-C16 PIP_2 and natural PIP_2.* ***(c)*** *Histogram with recovery current values with different phosphoinositides derivatives (modified from Ye et al., 2018).*

Mutagenesis studies showed that a stretch of positively charged amino acids in the N-terminus of the protein (K87, K88, K95, R96, K97, R98) were responsible for PIP_2-induced recovery after rundown. In mutants, where all these residues are neutralized, Ca^{2+} sensitivity and rundown were comparable with those of wild-type channels, but PIP_2 failed to revert the rundown and restore high Ca^{2+} sensitivity (Figure 8a, b, Figure 12).

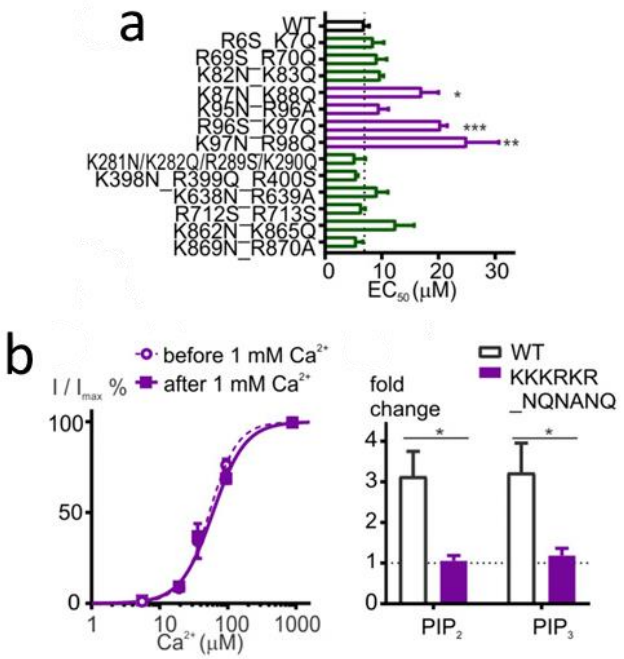

Figure 8. (a) *Ca^{2+} sensitivity of different mutants* ***(b)*** *Ca^{2+} sensitivity of mutant and effect of PIP_2 or PIP_3 on current recovery (modified from Ye et al., 2018).*

1.2.2.3. Ion selectivity

TMEM16F was first reported as an important element of the outwardly rectifying Cl^- Channel, which is an anion channel characterized by a non-linear current-voltage relationship. In the same report TMEM16F was knockdown with siRNA, and the outwardly rectifying Cl^- Channel activity induced by FasL in Jurkat T lymphocytes was dramatically decreased. Moreover, using BAPTA as chelator, it was shown that the outwardly rectifying Cl^- Channel activation was not Ca^{2+}-dependent (Martins et al., 2011).

Szteyn et al. (2012) showed that TMEM16F mediates a Ca^{2+}-dependent Cl^- current in dendritic cells. In fact, both ionomycin and IP_3 are able to induce TMEM16F-mediated Cl^- current activation (Szteyn et al., 2012).

In 2013, two groups recorded the ion selectivity in whole-cell configuration from HEK-293 expressing TMEM16F. They replaced Cl^- with aspartate in the bath solution, and measured a positive shift of the reversal potential respectively of +20 and +13 mV (Grubb et al., 2013; Shimizu et al., 2013). Both these values subtend an incomplete anion

selectivity of TMEM16F. Also Henkel et al. (2015), stimulating HEK-293 cells with ATP, detected anion currents activated by Ca^{2+}, indicating that TMEM16F carried Cl^- ions (Henkel et al., 2015)

Scudieri et al. (2015) studied the properties of four different isoforms of TMEM16F. Reducing NaCl concentration, they observed that all the TMEM16F variants

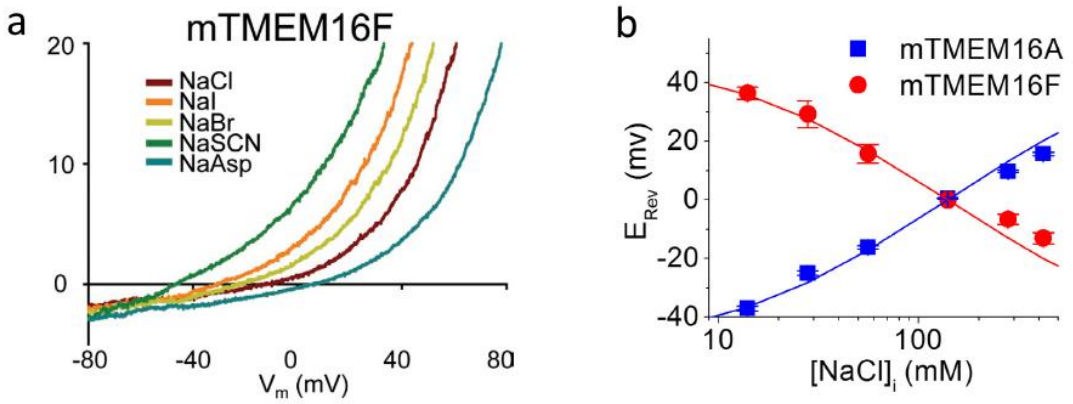

Figure 9. (a) *Whole-cell recordings showing I-V relationships of murine TMEM16F current upon perfusion of different Na salts (Grubb et al., 2013).* ***(b)*** E_{Rev} *values of TMEM16A and TMEM16F under different NaCl concentrations (Yang et al., 2012).*

showed a permeability ratio $P_{Na}/P_{Cl} \approx 0.5$, subtending a weak anion selectivity (Scudieri et al., 2015). Using a similar approach, Yu et al. (2015), by decreasing CsCl concentration, found that TMEM16F is a non-selective channel (Yu et al., 2015).

All these data are in contrast with the results from Yang et al. (2012), in which TMEM16F was found to be a cationic channel with a $P_{Na}/P_{Cl} = 7$. These data were obtained upon heterologous expression of TMEM16F in Axolotl oocytes or HEK-293 cells, and from native TMEM16F current in megakaryocytes. Interestingly, among all cations, they found that TMEM16F is more permeant to divalent cations, such as Ca^{2+} and Ba^{2+}. They also identified a glutamine residue, in the fifth transmembrane domain, which seems to be involved in ion selectivity. If this glutamine (Q559) is replaced with a lysine, TMEM16F shows a lower cation selectivity, with a $P_{Na}/P_{Cl} = 2.2$ (Yang et al., 2012).

1.2.3. Scramblase activity

1.2.3.1. Membrane asymmetry and lipid transporters

The cellular membrane has an asymmetrical distribution of lipids, with phosphatidylcholine (PC) and sphingomyelin (SM) mostly present in the external monolayer, while phosphatidylserine (PS), phosphatidylinositol (PI), and phosphatidylethanolamine (PE) are abundant in the inner side of the plasma membrane. This asymmetry is required in many physiological contests and it is obtained through the activity of the ATP-dependent flippases and ABC transporters. Flippases can move lipids from the external side to the cytosolic one, whereas ABC transporters work in both directions. Both proteins work against the chemical gradient using ATP as energy source. Another class of lipid transporters are the scramblases, which do not depend on ATP hydrolysis but are activated by the increase of the intracellular Ca^{2+} concentration. These proteins move lipids bidirectionally, following the lipid chemical gradient, disrupting the asymmetrical lipid localization (Coleman et al., 2013; Hankins et al., 2015; van Meer, 2011; Pomorski and Menon, 2006) (Figure 10).

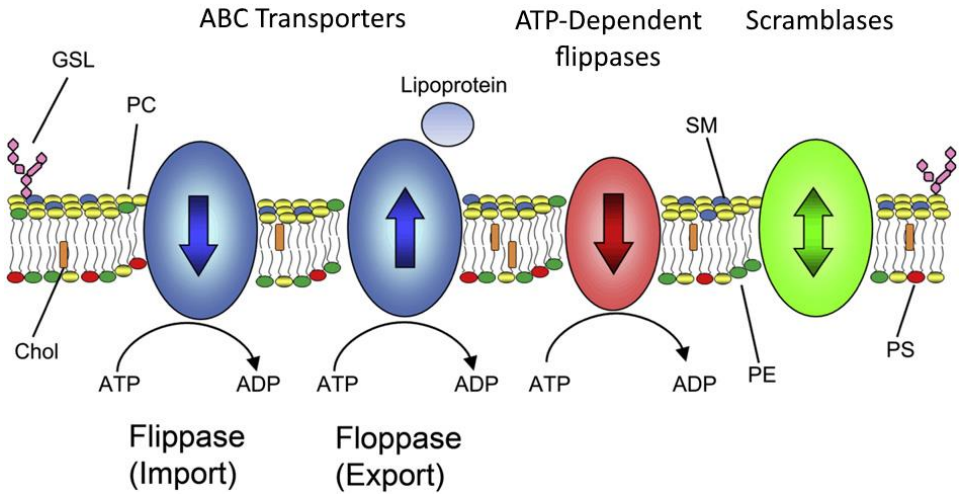

Figure 10. *Schematic representation of lipid transporters. In blue, ABC transporters, responsible for the ATP-dependent translocation of lipids between the cellular monolayers. In red, ATP-dependent flippases, which move lipids only toward the cytosolic membrane side. In green, scramblases, which do not require energy to display their function and translocate lipids both to outer and inner leaflet (modified from Coleman et al., 2013).*

Scramblase activity is correlated with a large spectrum of relevant physiological roles, such as PS exposure on platelets during coagulation, apoptosis and dying cell phagocytosis (Bevers and Williamson, 2010).

1.2.3.2. Identification of TMEM16F scramblase activity

In 2010, Suzuki et al. first identified TMEM16F as a scramblase. They detected endogenous Ca^{2+}-dependent scramblase activity in a murine B-cell line (Ba/F3), as these cells displayed PS exposure after treatment with Ca^{2+} ionophore. Thus, they selected a cell subline with the strongest PS exposure, constructed a cDNA library from this subline, and identified the cDNA responsible for scramblase activity by expression cloning. This cDNA encoded for a mutated version of TMEM16F (D409G, Figure 11). Thus, they expressed wild-type TMEM16F and the mutant isoform in Ba/F3 and HEK-293 cells. The results showed that the mutant TMEM16F induced a constitutive exposure of PS, whereas the wild-type TMEM16F was able to expose PS just after ionophore treatment. Furthermore, Suzuki et al. (2010) knocked down TMEM16F using short hairpin RNA and found a decreased PS exposure (Suzuki et al., 2010). These results were further confirmed by creating a $TMEM16F^{-/-}$ mouse lymphocyte cell line in which PS exposure was shown to be absent (Suzuki et al., 2013).

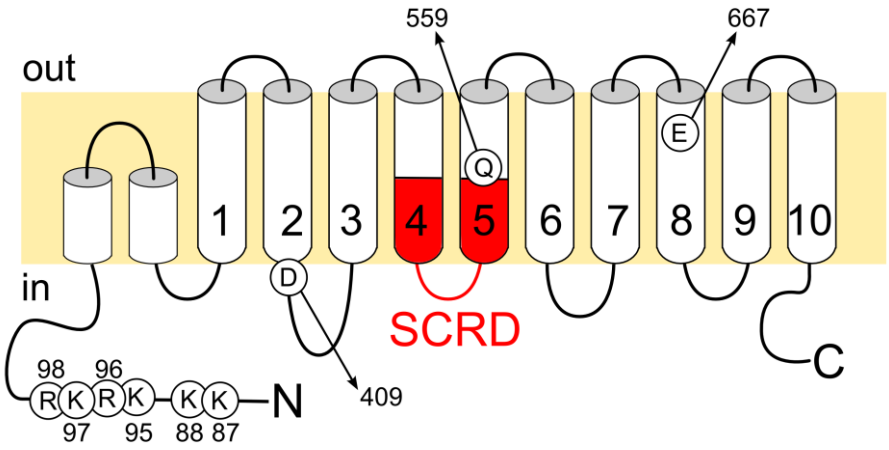

Figure 11. *TMEM16F topology based on the homology with TMEM16A. Models of topology of TMEM16F highlighting the localization of different residues controlling different TMEM16F properties (SCRS, Scrambling domain).*

1.2.3.3. Structure and possible mechanisms of scrambling

A proposed model for lipid translocation resembles the swiping of a card through a card reader (Pomorski and Menon, 2006). In this model the phospholipid headgroups (the magnetic strip on the card) diffuse through a hydrophilic path (the groove of the card reader), while the acyl chains remain in the hydrophobic regions of the membrane (Pomorski and Menon, 2006). The X-ray structure of nhTMEM16 confirmed the presence of a hydrophilic groove (Brunner et al., 2014). Indeed, nhTMEM16 is a dimer in which each subunit presents 10 TDs with a hydrophilic channel, which completely crosses the cellular membrane. This cavity, surrounded by 4 and 6 domains, is in contact with lipids and seems to be the best candidate to achieve lipid transport (Brunner et al., 2014, 2016).

Apresent, it is still unclear how Ca^{2+} ions can activate scrambling. Brunner et al. (2016), proposed three different hypothetical models for Ca^{2+}-dependent scramblase activation (Figure 12):

- Clogging: in the absence of Ca^{2+}, the hydrophilic groove blocks the subunit cavity preventing lipids translocation. Ca^{2+} ions induce the hydrophilic groove reorganization, which releases the subunit cavity and allows lipids transport.

- Plug: Ca^{2+} induces a movement of the cytoplasmic domains, which blocks the path in the inactive conformation, allowing lipids transport.

Electrostatic gate: no conformational change occurs. In the inactive conformation, the negative charges of Ca^{2+}-binding site could repel electrostatically the negative lipid headgroups. When the Ca^{2+} occupies its binding site, the negative charges are shielded; the electrostatic block is removed allowing the lipid translocation

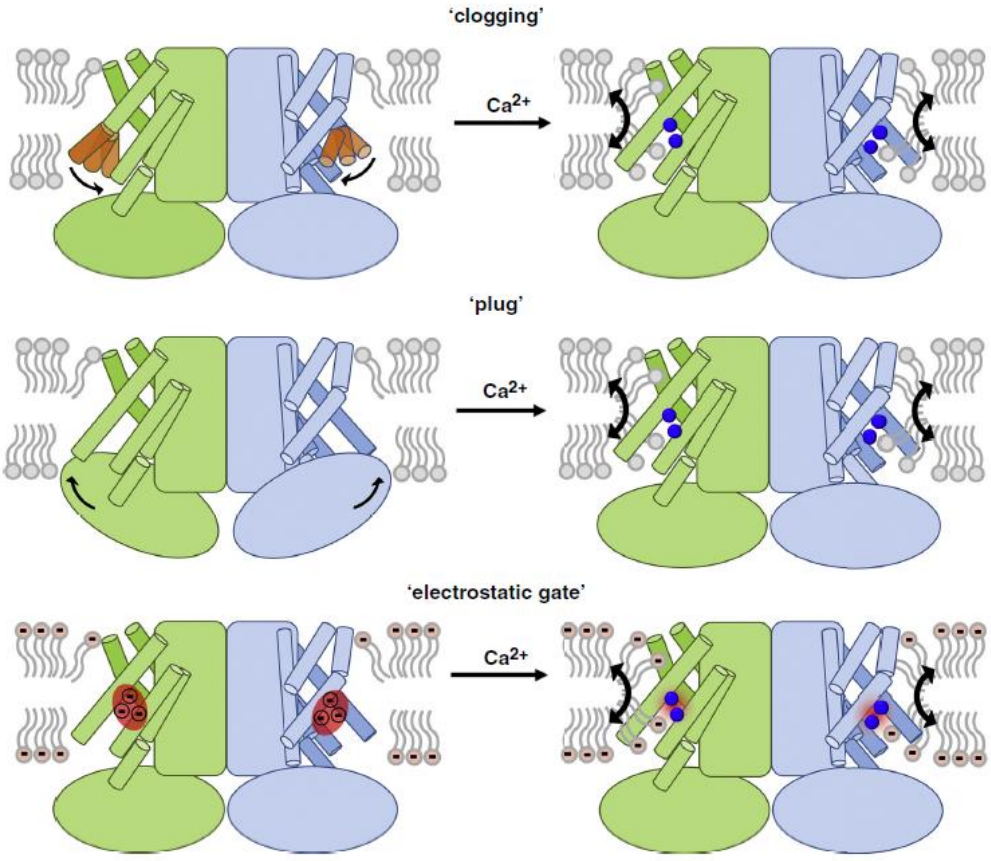

Figure 12. *Models of mechanisms for Ca^{2+} activation. Inactive or active proteins are shown respectively on the left or on the right. Blue spheres represent Ca^{2+}. Top, 'clogging', Ca^{2+} binding produces a conformational change in the subunit cavity. Center, 'plug', Ca^{2+} binding allows the movement of cytoplasmic domains that were keeping the path in the inactive conformation. Bottom, 'electrostatic gate', binding of Ca^{2+} neutralizes the negative net charge in the binding site (red) removing an electrostatic barrier and allowing lipids to cross the cavity (Brunner et al., 2016)*

The authors also proposed that these three models could coexist (Brunner et al., 2016).

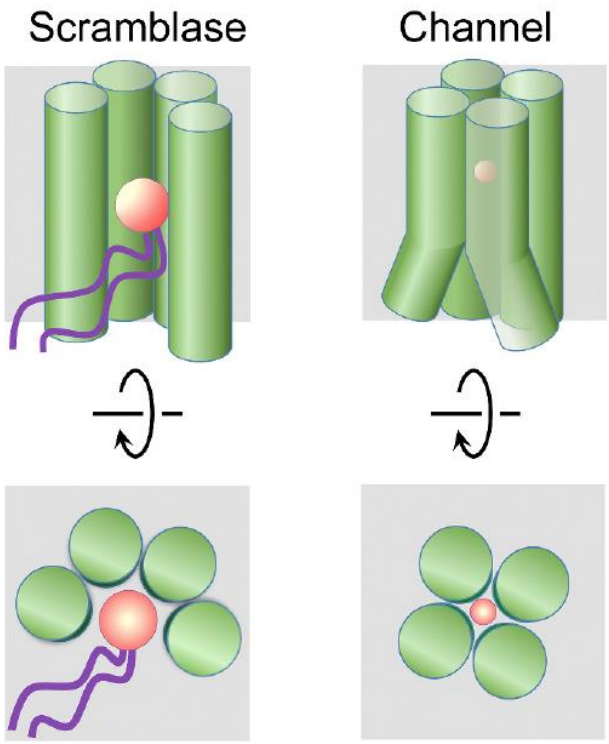

Figure 13. *Schematic representation of the structural difference between lipid scramblases (left) from ion channels (right) in the TMEM16 family. The view is from inside the membrane (top panels) and from the top (bottom panels). The transmembrane domains forming the site of catalysis in scramblases are closer in TMEM16 channels, forming the pore. Permeating ions and lipid headgroups are indicated in red (apulino et al., 2017).*

What are the structural differences between ion channels and scramblases in the TMEM16 family? Paulino et al. (2017b) reported that the general structures of mTMEM16A and nhTMEM16 are largely similar. The main difference is a rearrangement of TD4 and TD6, which are closer in TMEM16A, occluding the lipid pathway and creating a conductive pore. The authors also reported that the intracellular regions of TD4 and TD6 are detached, forming a vestibule exposed to the lipid bilayer (Figure 13). They suggested that this vestibule could be a relic of an ancestral scramblase (Paulino et al., 2017b).

All TMEM16 proteins share a Ca^{2+} binding site, composed of highly conserved amino acids in 6, 7 and 8 TDs. These residues are very important not only for TMEM16A Ca^{2+} gating (Dang et al., 2017; Paulino et al., 2017a; Tien et al., 2014; Yu et al., 2012), but

also for scrambling regulation in TMEM16 fungal homologous (Brunner et al., 2014; Malvezzi et al., 2013).

Recently, Lee et al. (2018) expanded the information about the mechanisms underlying TMEM16 scrambling. In nhTMEM16, replacing the residues facing the hydrophilic groove with tryptophan, they detected that several mutations impaired scramblase activity. These crucial amino acids are located in three distinct portions of the hydrophilic groove: the extracellular constriction (E313 and R432), the groove mid-point constriction (L302, T340, T381 and S382) and the area between the two constrictions (A385, Q436, Y439 and F440). They also showed that lipids surrounding the extracellular entrance are involved in the opening of the groove and the subsequent lipids movement. They proposed a model in which lipid headgroups interact with three charges residues (E313, R432 and E318), triggering their reorganization, opening the groove and allowing lipid scrambling. Moreover, they found that most of these mutations affected also ion channel activity. All these data appear to suggest that the same amino acids play an important role in controlling both ion and lipid movements, subtending a shared pathway (Lee et al., 2018).

1.2.3.4. Relationship between scramblase and channel activities

The relationship between phospholipid scrambling and ion conduction is unclear. Indeed, although nhTMEM16, afTMEM16 and TMEM16F show Ca^{2+}-activated currents, the physiological role of these currents remains unclear (Grubb et al., 2013; Lee et al., 2016; Malvezzi et al., 2013; Shimizu et al., 2013; Yang et al., 2012).

The scramblase function does not seem to be affected by the current carried by the protein. Using Cl^- blockers or reducing the Cl^- concentration the TMEM16F scramblase function is not affected (Kmit et al., 2013). Moreover, afTMEM16 scrambling is unaffected by different ions and even by ion transport inhibition (Malvezzi et al., 2013). Whitlock et al. (Whitlock and Hartzell, 2016), proposed that the TMEM16F current is just a leak current produced by lipid translocation. The authors suggested that ion conduction and lipid transport pathways occur in the same protein region and because of that, part of the channel is actually composed of lipids (Whitlock and Hartzell, 2016).

A similar idea has been proposed by Yu et al. (2015). They found that the TMEM16F current and scrambling activity shared a similar time of activation and kinetics, supporting the idea that the TMEM16F current is a “collateral” effect of lipids scrambling. Interestingly, analyzing TMEM16A-TMEM16F chimeric proteins, they identified a domain in TMEM16F sufficient for Phopholipids scrambling to generate scramblase activity in TMEM16A, which normally does not scramble (Yu et al., 2015). Gyobu et al., (2017) obtain similar results, producing different chimeras composed of TMEM16A and the scrambling domain of other TMEM16 family members (C, D, E, F, G, H and J; Gyobu et al., 2017).

2. Project aims

The specific aims of this work were:

- To provide an electrophysiological characterization of TMEM16F-mediated currents.

- To compare the ionic selectivity of TMEM16F current in different recording conditions.

- To investigate the role a specific amino-acid residue in controlling the ionic selectivity of TMEM16F.

3. Materials and Methods

3.1. Cell culture and transfection

HEK293T cells were grown in medium composed DMEM (Gibco, Italy) supplemented with 10% fetal bovine serum (Sigma, Italy), 100 UI/ml penicillin and 100 µg/ml streptomycin (Sigma, Italy) at 37 °C in humidified atmosphere of 5% CO_2.

Plasmid pEGFP-N1 containing the cDNA of mouse TMEM16F (version 1 as in Scudieri et al., 2015) wt or Q559K mutant was provided by Dr. Lily Jan (UCSF, USA). HEK293T cells were transfected with 2 µg TMEM16F cDNA using transfection reagent XtremeGENE (Roche diagnostic, USA).

After 24 h from transfection the cells were subcultured at lower density to 35-mm petri dishes (Thermo Scientific, USA). Electrophysiological recordings were performed between 48-72 h from transfection.

3.2. Electrophysiological recording

HEK293T cells were visualized under an Olympus IX70 inverted microscope (Olympus, Japan) placed on anti-vibration table (TMC, USA) and protected from external noise by a homemade Faraday cage. All the instruments kept inside the Faraday cage were connected to a single ground to avoid current loops.

TMEM16F currents were recorded in whole-cell or inside-out configuration using a Axopatch 1-D amplifier controlled by Clampex 9.2 via Digidata 1322A (Axon Instruments, USA). The data was acquired at rate of 10 kHz and the signals were lowpass filtered at 5 kHz.

Patch electrodes were made of borosilicate glass (WPI, USA) and pulled with a PP-830 micropipette puller (Narishige, Japan). Pulled patch electrodes had resistance of 2-3 MΩ for whole-cell and 0.5-1 MΩ for inside-out configuration when filled with pipette solution.

The patch electrode was mounted on electrode holder with Ag/AgCl electrode, connected to CV-4 headstage (Axon Instrument, USA). The movement of the headstage was controlled by MM3 mechanical micromanipulator (Narishige, Japan) for coarse

movement and through MWO-3 three dimensional oil hydraulic micromanipulator (Narishige, Japan) for fine adjustment.

The bath was grounded with a 3 mM KCl agar bridge connected with Ag/AgCl reference electrode. All the experiments were conducted at room temperature.

3.3. The perfusion system

Solutions were rapidly changed close to the cells or excised patches by using a multi-barrel glass tube. Each tube composing the multi-barrel has an internal diameter of 0.9 mm (Vitro Dynamics, USA). Changes between different solutions were performed by using the Perfusion Fast-Step SF-77B (Warner Instrument Corp., USA) that could be controlled both manually or automatically by the Digidata 1322A (Axon Instruments, USA). The perfusion system was entirely gravity driven.

The solutions were stored in 50 ml syringes and polyethylene tubes (ID 1.14 mm) were used for connection with the perfusion system and the recording chamber. The flow of each solution was manually controlled with a stopcock.

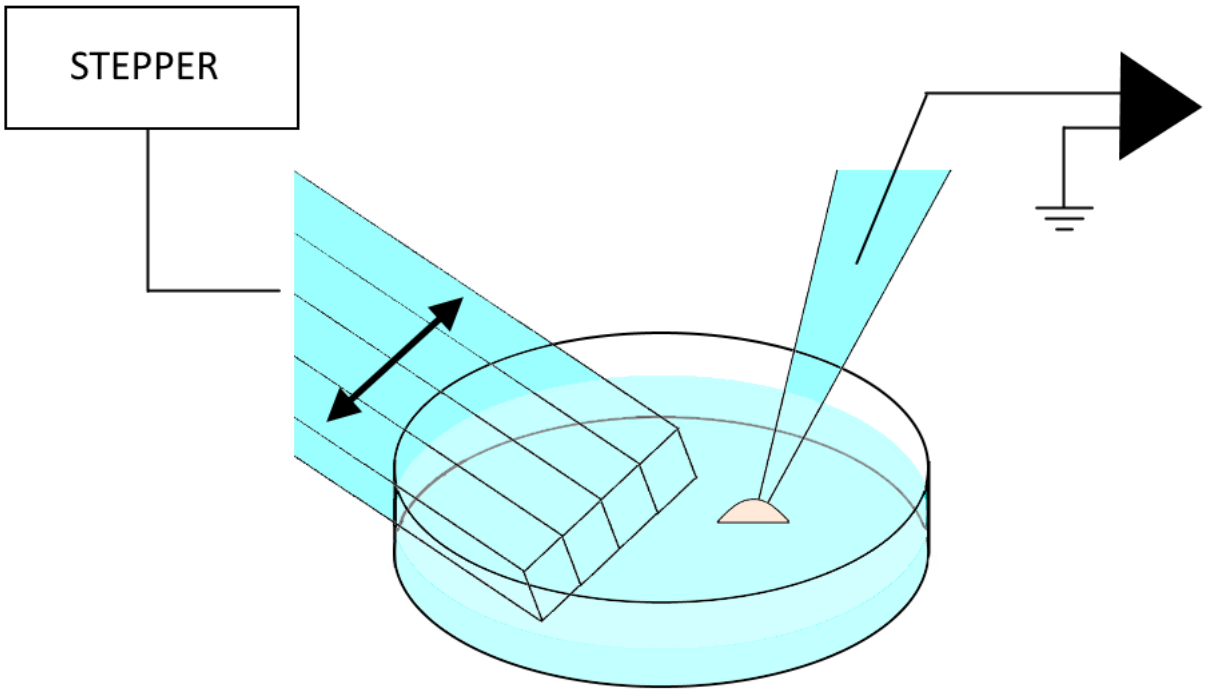

Figure 13. *Schematic representation of perfusion system. Four parallel streams of solutions emerging from glass pipes were delivered in front of the patch pipette. Through motorized movement of pipes, it was possible to change rapidly the solutions bathing the cells or the excised patch.*

During experiments, cells were constantly perfused with Ringer's solution, while an aspiration tube, connected to a suction pump, was used to maintain constant the level of Ringer's solution.

3.4. Solutions

The extracellular mammalian Ringer solution was composed of (in mM) 140 NaCl, 5 KCl, 2 $CaCl_2$, 1 $MgCl_2$, 10 glucose (to adjust the osmolarity) and 10 HEPES (to buffer the pH). Mammalian Ringer's solution was applied extracellularly in the bath, while solutions with different free Ca^{2+} concentrations were used as intracellular solutions, both in whole cell and inside-out recordings. These solutions were composed as reported in the following table:

Free Ca^{2+} (µM)	***NaCl (mM)***	***$CaCl_2$ (mM)***	***HEDTA (mM)***	***HEPES (nM)***
1.5	140	3.21	10	10
3.8	140	5.86	10	10
13	140	8.26	10	10
30	140	9.26	10	10
50	140	9.57	10	10
100	140	9.98	10	10

Free calcium concentrations, contained in different solutions, have been calculated using WINMAX C (C. Patton, Stanford university, Palo Alto, CA USA) (Patton et al., 2004). Osmolarity for all the solutions were balanced in range of 280-300 mOsm with glucose. The pH of the solutions was adjusted with NaOH reaching a value of 7.4 for extracellular solutions and 7.2 for intracellular solutions.

3.5. Data analysis

The electrophysiological recordings were saved as *.abf* file in Clampex 9.2 (Axon Instruments, USA), and subsequently analyzed using IGOR Pro software (Wavemetrics, Lake Oswego, OR, USA). IGOR procedures used for analysis were written both by Dr. Simone Pifferi and myself. All the figures presented in the Results have been prepared using IGOR.

Data are presented as mean ± SEM, with n indicating the number of cells. Statistical significance was determined using paired t-tests or ANOVA as appropriate. When a statistically significant difference was determined with ANOVA, a post hoc Tukey test was done to evaluate which data groups showed significant differences. P values < 0.05 were considered significant.

4. Results

(Manuscripst in preparation)

"Anion and cation permeabilities of the mouse TMEM16F/ANO6 calcium-activated channel"

Stefano Stabilini, Anna Menini and Simone Pifferi

Neurobiology Group, SISSA, International School for Advanced Studies, Trieste, Italy

Abstract

TMEM16F/ANO6 is widely expressed in different tissues where it plays important physiological roles, such as the regulation of blood coagulation and apoptosis. TMEM16F has a dual function, indeed it acts both as Ca^{2+}-dependent scramblase and as Ca^{2+}-activated ion channel. Scramblases are integral membrane proteins responsible for the translocation of phospholipids between the two leaflets of a lipid bilayer upon their electrochemical gradient. Many studies investigated in details the molecular mechanisms of TMEM16F lipid scrambling and identified a specific domain of the protein necessary for the lipid transport. In contrast, the mechanisms of ion channel activity are less clear and, in particular, several studies reported conflicting results about the ionic selectivity of the TMEM16F-mediated current. These data were partially obtained using different methodologies and analysis making difficult to reconcile the discrepancies. Here we decided to investigate the ionic selectivity of TMEM16F using two configurations of the patch clamp technique, whole-cell and inside-out excised patch, in order to directly compare the results. Moreover, we investigated the properties of the Q559K mutant that has been reported to alter the ionic selectivity of TMEM16F in inside-out patches. TMEM16F heterologous expression in HEK 293T cells generates a large outward rectifying Ca^{2+}-activated current both in whole-cell and inside-out configuration. This rectification is due to the voltage-dependent gating of the channel. In inside-out experiments the Ca^{2+}-dependent activation is fast and the TMEM16F-mediated current is activated in few ms, while in whole-cell recordings a full activation requires up to 4 minutes. Similar results are obtained also with Q559K mutant. In inside-out patches the Ca^{2+} concentration for half-maximal current activation ($K_{1/2}$) is 42 µM at +60 mV, while the Hill coefficient is >2. Q559K mutant shows a significant reduction of Ca^{2+} sensitivity with a $K_{1/2}$ almost 5-folds higher and a reduction of Hill coefficient to 1.4, indicating a possible alteration of the gating mechanism. We determined the relative permeability between Na^+ and Cl^- (P_{Na}/P_{Cl}) using the dilution method both in whole-cell and inside-out configuration. TMEM16F-mediated current is highly non-selective but there are differences depending on the configuration of the recordings. In whole-cell both TMEM16F wild type and the mutant Q559K have a P_{Na}/P_{Cl} around 0.5 indicating a slight preference for Cl^- permeation. In contrast, in inside-out experiments the Q559K mutant retains a higher permeability for Cl^-, while TMEM16F wild type channel shows a higher permeability for Na^+ with a P_{Na}/P_{Cl} reaching 3.6. These results have two major implications: first the ionic selectivity of the TMEM16F wild type is controlled by a soluble factor, which is lost in the inside-out configuration; second the residue in position 559 controls the selectivity among cations and anions when this soluble factor is lost.

Introduction

TMEM16 family is a group of proteins presents in all the eukaryotic organism and in mammalians is composed of 10 members (TMEM16A-K). The two first members of this family, TMEM16A and TMEM16B, have been characterized as Calcium-activated Chloride Channels (CaCC), respectively in 2008 (Caputo et al., 2008; Schroeder et al., 2008; Yang et al., 2008) and 2009 (Pifferi et al., 2009; Stephan et al., 2009; Stöhr et al., 2009). TMEM16A and TMEM16B are involved in fluid secretion, neuronal and smooth muscle cells excitability, olfaction and photo-transduction (Bulley et al., 2012; Caputo et al., 2008; Danahay et al., 2002; Davis et al., 2010, 2013; Galietta et al., 2002; Huang et al., 2012; Manoury et al., 2010; Rasche et al., 2010; Stephan et al., 2009; Stöhr et al., 2009; Thomas-Gatewood et al., 2011).

Recently, two different papers predicted the structure of TMEM16 family members, based on the mouse TMEM16A structure, obtained by cryogenic electron microscopy. They found a homodimeric structure, with subunits composed of 10 transmembrane domains (TM), with cytosolic N- and C-terminal. Each subunit contains an ion conducting pore, surrounded by TM3-TM7. They also found that TM6 is important in the channel gating (Dang et al., 2017; Paulino et al., 2017).

TMEM16F is another member of the TMEM16 family, which is broadly expressed in different tissues, such as bones, skin, lungs, muscles, kidney, pancreas, thyroid, blood cells, etc. (Ehlen et al., 2013; Schreiber et al., 2010; Scudieri et al., 2015; Shimizu et al., 2013).

TMEM16F is linked with scramblase activity. The scramblases are proteins able to translocate lipids between the two leaflets of the membrane. In normal condition, the cellular membrane has an asymmetric distribution of lipids, maintained by different ATP-dependent proteins. When the intracellular Ca^{2+} concentration increases, the scramblases are activated and translocate lipids following the chemical gradient, dissipating the asymmetry of cellular membrane (Coleman et al., 2013; Hankins et al., 2015; van Meer, 2011; Pomorski and Menon, 2006). During this process Phosphatidylserine (PS) is translocated from the inner side, where it is present in resting conditions, to the external side of the plasma membrane. The PS exposition is a key process involved in several physiological functions played by TMEM16F, such as coagulation (Baig et al., 2016; van Kruchten et al., 2013; Yang et al., 2012), immunity (Ousingsawat et al., 2015) and apoptosis (Brooks et al., 2015; Kmit et al., 2013; Schenk et al., 2016).

Moreover, TMEM16F has been correlated also with channel activity. Initially, TMEM16F has been reported as an important element of the Outwardly Rectifying Cl^- Channel (ORCC), which is an anion channel characterized by non-linear current-voltage relationship (Martins et al., 2011). Other groups reported that TMEM16F is a CaCC. Other groups reported that TMEM16F is a CaCC. Unlike TMEM16A and TMEM16B, the calcium sensitivity of

TMEM16F and the chloride permeability is lower (Grubb et al., 2013; Shimizu et al., 2013; Szteyn et al., 2012). Also Henkel et al. (2015), detected anion currents activated by Ca^{2+}, but with Ca^{2+}-sensitivity in sub-micromolar range (Henkel et al., 2015). Finally, Scudieri et al. (2015) and Yu et al. (2015), changing Cl^- concentration, found that TMEM16F is a non-selective channel (Scudieri et al., 2015; Yu et al., 2015).

All these data are in contrast with the findings from Yang et al. (2012). They reported that TMEM16F is a channel with single-channel conductance of 0.5 pS, which is more permeable for cations than anions and specifically for Ca^{2+} and Ba^{2+} with $P_{Na}/P_{Cl} = 7$. They also identified a glutamine residue, in the fifth transmembrane domain, which seems to be involved in ion selectivity. Replacing glutamine (Q559) with a lysine, TMEM16F shows a lower cation selectivity, with a $P_{Na}/P_{Cl} = 2.2$ (Yang et al., 2012).

Here, we are presenting a complete picture regarding TMEM16F selectivity, analyzing the channel activity both in inside-out and whole-cell configuration, with the aim of clarifying the controversial selectivity of this channel.

Materials and Methods

Cell culture and transfection

HEK-293 cells were grown in medium composed by DMEM (Gibco, Italy) supplemented with 10% fetal bovine serum (Sigma, Italy), 100 IU/ml penicillin and 100 μg/ml streptomycin (Sigma, Italy) at 37 °C in humidified atmosphere of 5% CO_2.

Plasmid pEGFP-N1 containing the cDNA of mouse TMEM16F wt (version 1 as in Scudieri et al., 2015) or Q559K mutant was provided by Dr. Lily Jan (UCSF, USA). HEK-293 cells were transfected with 2 μg TMEM16F cDNA using the transfection reagent XtremeGENE (Roche diagnostic, USA). After 24 h from transfection the cells were subcultured at lower density to 35-mm petri dishes. Electrophysiological recordings were performed between 48-72 h from transfection.

Electrophysiological recordings

TMEM16F HEK-293 transfected cells were identified by EGFP fluorescence using an Olympus IX70 microscope (Olympus, Japan) equipped with appropriate filter. TMEM16F currents were recorded in whole-cell or inside-out configurations in voltage clamp mode using a Axopatch 1-D amplifier controlled by Clampex 9.2 via Digidata 1322A (Axon Instruments, USA). The data was acquired at rate of 10 kHz and the signals were low pass filtered at 5 kHz. Patch electrodes were made of borosilicate glass (WPI, USA) and pulled with a PP-830 micropipette puller (Narishige, Japan). Pulled patch electrodes had resistance of 2-3 MΩ for whole-cell and 0.5-1 MΩ for inside-out configuration when filled with pipette solution.

The bath was grounded with a 3 M KCl agar bridge connected with Ag/AgCl reference electrode. In experiments with pipette solution without Cl^- a 3 M KCl agar bridge was used. All the experiments were conducted at room temperature. Solutions were rapidly changed close to the cells or excised patches by using multi-barrel glass tubes. Each tube composing the multi-barrel had an internal diameter of 0.9 mm (Vitro Dynamics, USA). Changes between different solutions were performed by using the Perfusion Fast-Step SF-77B (Warner Instrument Corp., USA).

For IV relations in the inside-out configuration, we exposed the patches to Ca^{2+}-containing solution for 1 s at +100 mV and then we applied a ramp from +80 to -80 mV at 0.36 mV/ms. Leak currents measured in normally 0 Ca^{2+} solution were subtracted. The reversal potential (E_{rev}) was estimated by using a fit with a polynomial function.

In whole-cell recordings the IV relations were determined by using a voltage ramp protocols or by measuring tail currents. Voltage ramps were applied from +100 to -100 mV at 0.2 mV/ms after a depolarization at +100 for 1 s. For tail currents, the protocol consisted of voltage steps of 500 ms duration from a holding potential of 0 mV to + 80 mV followed by voltage steps ranging from -20 to +50 mV. A single-exponential function was fitted to tail currents to extrapolate the tail current value at the beginning of the step. Tail current values were plotted as a function of voltage, and E_{rev} was estimated using a fit with a polynomial function. Liquid junction potentials were calculated using pClampex software (Axon Instruments, USA) and applied voltages were corrected off-line.

Solutions

Cells were kept in mammalian Ringer's solution composed of (in mM): 140 NaCl, 5 KCl, 2 $CaCl_2$, 1 $MgCl_2$, 10 glucose and 10 Hepes, pH 7.4 with NaOH.

For whole-cell recordings, the pipette solution contained (in mM): 140 NaCl, 10 Hepes, 10 HEDTA, pH 7.2 and 5.86, 8.26 or 9.26 mM $CaCl_2$ to obtain 3.8, 13 or 30 µM free Ca^{2+}, respectively. For intracellular solutions containing Ca^{2+} concentrations >50 µM, HEDTA was omitted and appropriate amount of $CaCl_2$ was used. For permeability experiments, cells were bathed with solution containing (in mM): 140 NaCl, 10 Hepes, pH 7.4. NaCl was reduced to 14 mM or substituted with NaMeS (sodium methanesulfonate), or NaSCN. The osmolarity in low NaCl solution was adjusted with sucrose.

For inside-out recordings, the pipette solution contained (in mM): 140 NaCl (or NaMeS), 5 EGTA, 10 Hepes, pH 7.2 with NaOH. The patches were maintained in nominally 0 Ca^{2+} solution containing (in mM): 140 NaCl (or NaMeS if used in the pipette solution), 10 HEDTA or 5 EGTA, 10 Hepes, pH 7.2. For dose-response relations the bath solution was the same used in the pipette for whole-cell recordings. For permeability experiments using the dilution methods the bath solution contained (in mM): 140 NaCl, 10 Hepes, 0.1 or 1 mM $CaCl_2$ and NaCl was changed to 280, 70, 28, or 14 mM. The osmolarity in low NaCl solution was adjusted with sucrose. For anion selectivity, Cl^- was substituted with other anions by replacing NaCl on an equimolar basis with NaX, where X is the substituted anion. Similarly, for cation selectivity experiments Na^+ was substituted with other cations by replacing NaMeS on an equimolar basis with YMeS, where Y is the substituted cation. All chemicals were purchased from Sigma-Aldrich (Milano, Italy).

Data analysis

Data analysis and figures were made with IgorPro software (Wavemetrics, Lake Oswego, OR, USA). Data are presented as mean ± SEM, with n indicating the number of cells. In the box plots the lines represent the median, the upper and lower box boundaries represent the 25^{th} and 75^{th} percentile, and upper and lower whiskers represent the 10^{th} and 90^{th} percentiles. Normality of the data was tested with Shapiro-Wilk test, while the homogeneity of variance was tested with Levene's test. Statistical significance was determined using paired U-test, t-tests or ANOVA as appropriate. When a statistically significant difference was determined with ANOVA, a post hoc Tukey test was done to evaluate which data groups showed significant differences. p values < 0.05 were considered significant.

Results

Ca^{2+} activation of TMEM16F current in whole-cell recordings.

Previous results show that in whole-cell recordings TMEM16F-mediated current developed slowly after the membrane breaking (Grubb et al., 2013; Scudieri et al., 2015; Yu et al., 2015). Therefore, we decided to measure the development of the current with time. We dialyzed TMEM16F wt or Q559K mutant-expressing HEK-293 cells with a pipette solution containing 300 µM of Ca^{2+} and we recorded the current induced by repeated voltage steps to +80 mV applied every 20 s from the holding potential of 0 mV (Fig. 1 AB). Both TMEM16F wt or Q559K mutant channels showed a gradual increase of current amplitude after membrane breaking reaching a steady state level after about 4 minutes (n= 8-21, p>0.05 U-test; Fig. 1 BC).

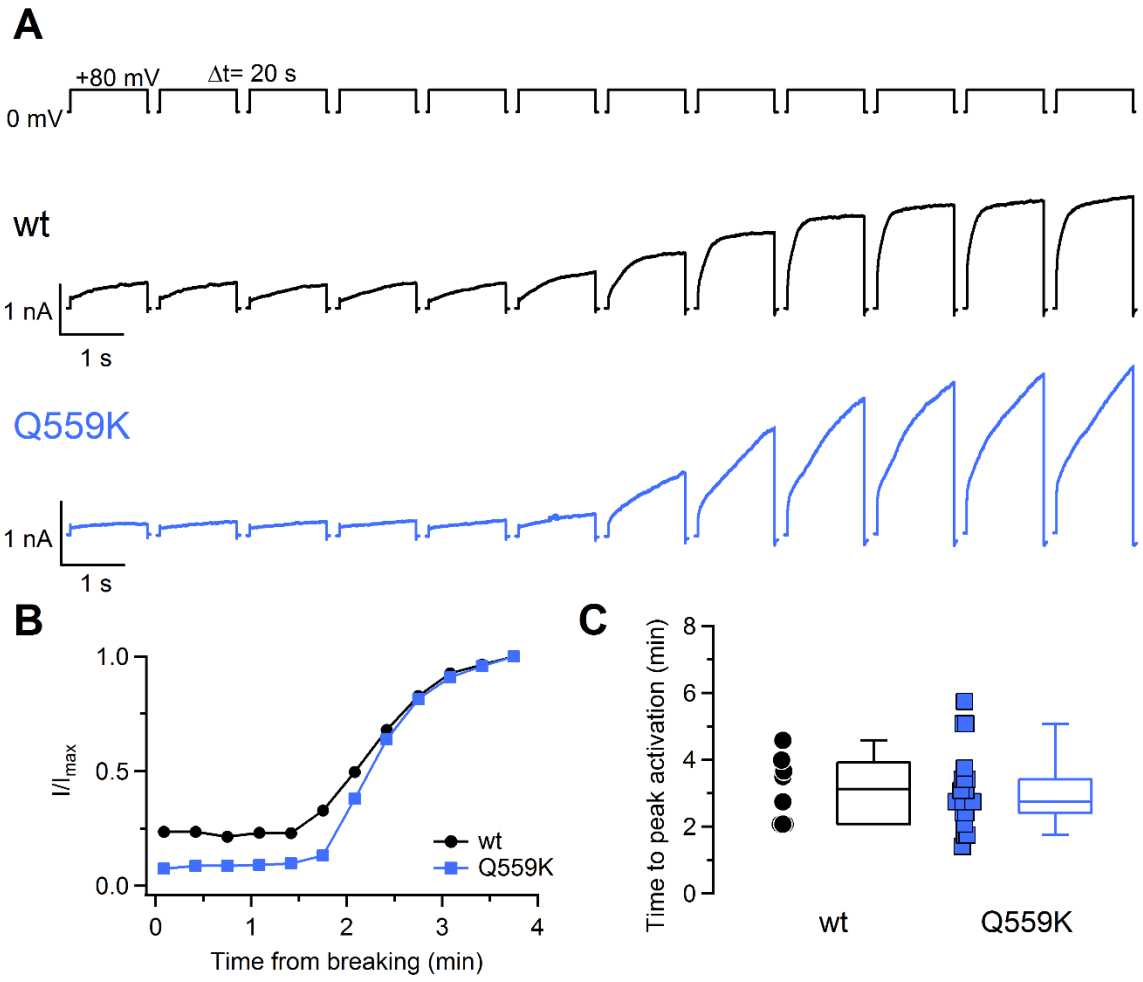

Figure 1. Time course of Ca^{2+}-activation kinetics of TMEM16F in whole-cell recordings. (A) Whole-cell recordings obtained from TMEM16F wt or Q559K mutant HEK 293 transfected cells with a pipette solution containing 300 μM Ca^{2+}. The current development was monitored by the application of +80 mV voltage step every 20 s as indicated in the upper traces. (B) Current amplitudes at the end of voltage steps were plotted against the time after membrane breaking for the recordings in (A). (C) Comparison of the time required to obtain the maximal current in TMEM16F wt or Q559K mutant transfected cells (n=8-21).

To determine the Ca^{2+} sensitivity of TMEM16F-mediated current we performed whole cell voltage-clamp using intracellular solutions containing different free Ca^{2+} concentrations. Figure 2 A shows currents activated by steps of 2.5 s duration given from a holding potential of 0 mV from -100 mV to +100 mV in 20 mV interval. The average current density in the presence of 3.8 μM of Ca^{2+} was 61 ± 15 pA/pF (n=6) significantly smaller than 338 ± 36 pA/pF and 254 ± 36 pA/pF recorded with 100 or 500 μM intracellular Ca^{2+} respectively (n=6-8 $p<0.01$ Tukey test after one way ANOVA $F=18.744$ $p=5*10^{-5}$; Fig. 2B). In contrast with the results obtained with TMEM16A and 16B (Caputo et al., 2008; Pifferi et al., 2009; Schroeder et al., 2008; Yang et al., 2008), we did not observe a significant change in the rectification depending on intracellular Ca^{2+} with a strong outward rectification at every Ca^{2+} concentration. The ratio between the current measured at the end of voltage pulses at +100 and -100 mV was 22 ± 8 (n=6) in the presence of 3.8 μM Ca^{2+} and 20 ±13 with 100 μM (n=7, p=0.28 U-test) respectively. To analyze the Ca^{2+} dependence of TMEM16F activation at various voltages, we plotted the average of the current density measured at the end of voltage pulse versus $[Ca^{2+}]_i$ and we fitted the data with the Hill equation $D = D_{max}[c^n_H/ (c^n_H + K_{1/2}{}^n_H)]$, where c is the Ca^{2+} concentration, $K_{1/2}$ the Ca^{2+} concentration producing half-maximal current activation, and n_H is the Hill coefficient (Fig. 2C). $K_{1/2}$ slightly decreased with membrane depolarization from 22.2 μM at +60 mV to 17.4 μM at +100 mV, while the Hill coefficient ranged from 1.6 to 3.8.

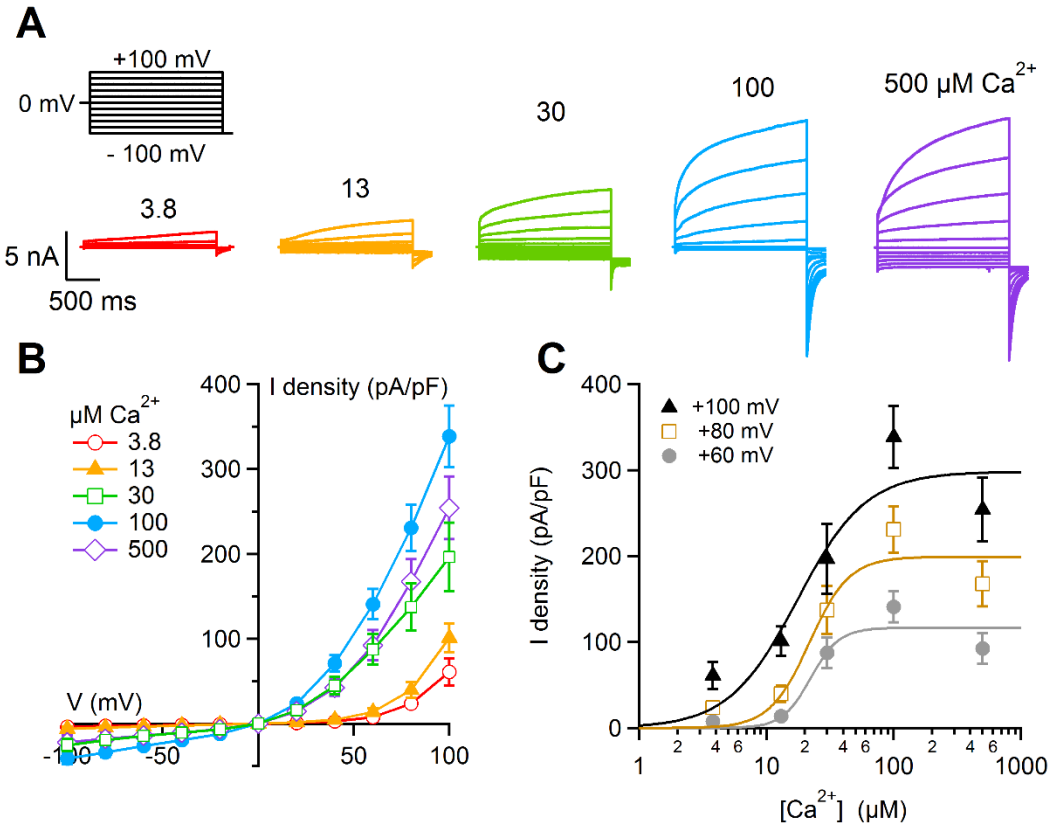

Figure 2. Ca^{2+} sensitivity of TMEM16F-mediated current in whole-cell recordings. (A) Representative whole-cell currents recorded from TMEM16F-expressing cells with a pipette solution containing the indicated intracellular [Ca^{2+}]. The voltage protocol is shown at the top of panel. (B) Average steady-state IV relationships from several cells at the indicated [Ca^{2+}]$_i$ (n =4-10). (C) Average ± sem of the current density was plotted against the intracellular [Ca^{2+}] (n =5-10). The continuous line is the fit with Hill equation.

Ionic selectivity in whole-cell recordings.

To investigate the ionic selectivity of TMEM16F-mediated current in whole-cell recordings we used the dilution method (Barry, 2006). We activated the current with 50 µM Ca^{2+} for TMEM16F wt or with 300 µM Ca^{2+} for Q559K mutant, changed the NaCl concentration in the bath solution from 140 mM to 14 mM, and measured the reversal potential (V_{rev}). To obtain a better estimate of V_{rev}, we measured tail currents after a prepulse at +80 mV of 500 ms duration (Fig. 3 A-C). Reduction of NaCl in the extracellular solution caused a positive shift of V_{rev} both for TMEM16F wt and Q559K mutant expressing cells. Relative permeability ratio between Na^+ and Cl^- (P_{Na} /P_{Cl}) calculated with the Goldman–Hodgkin–Katz equation was 0.52 ± 0.03 (n=7) for the wt channel, not significantly different from 0.41 ± 0.04 (n=8) for Q559K mutant ($p>0.05$ t-test). These data show that the TMEM16F wt and Q559K mutant channels recorded in whole-cell configuration were relatively unselective with Cl^- more permeant than Na^+ (Fig 3 E).

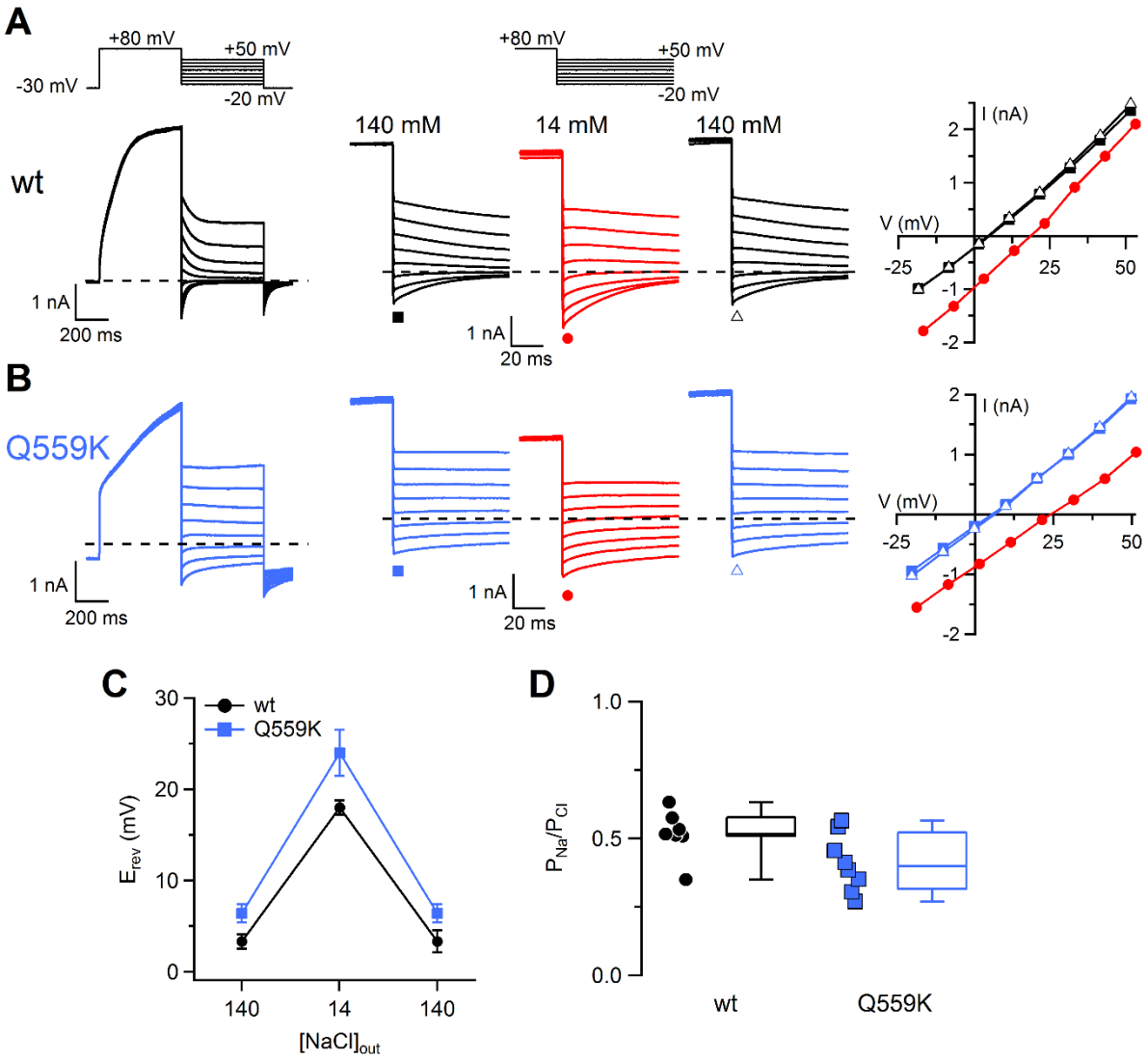

Figure 3. Ion selectivity of TMEM16F-mediated current in whole-cell recordings. (A-B) Representative whole-cell voltage-clamp recordings obtained from TMEM16F wt or Q559K mutant-transfected cells with intracellular solution containing 50 µM (wt) or 300 µM Ca^{2+} (Q599K mutant). The voltage protocol is shown at the top part of the panels. Each cell was exposed to a control solution containing 140 mM NaCl then to 14 mM NaCl, followed by wash out with 140 mM NaCl. I-V relations measured from tail currents for the cells shown on the left in 140 mM NaCl (squares), 14 mM NaCl (circles) and after the wash out (triangles). (C) E_{rev} corrected for liquid junction potential was plotted versus $[NaCl]_{out}$ for TMEM16F wt or Q559K transfected cells (n = 7-8). (D) Comparison of the permeability ratio between Na^+ and Cl^- (P_{Na}/P_{Cl}) in TMEM16F wt or Q559K mutant-transfected cells calculated with Goldman-Hodgkin-Katz equation (n=7-8).

In order to determine the anion selectivity of TMEM16F-mediated current in whole-cell recordings, we replaced NaCl in the extracellular solution with Na salts of different anions. The reversal potential was determined using a voltage ramp from -100 to +100 mV (Fig. 4 A).

We calculated relative permeability ratios between different anions and Na^+ (P_X /P_{Na}) with the Goldman–Hodgkin–Katz equation taking also into account the Na^+ permeability measured with the dilution method (Fig. 3). TMEM16F wt and Q559K mutant channel were equally permeable to methanesulfonate with permeability ratios of 0.42 ± 0.07 (n=5) for wt, and 0.53 ± 0.04 (n=26, p>0.05 t-test) for Q559K. In contrast, the Q559K mutant had a significantly higher permeability to SCN than TMEM16F wt channel (5.9 ± 0.3 n= 6 for wt , 8.3 ± 0.04 n=15 for Q559K, p=0.00012 t-test, Fig. 4 B).

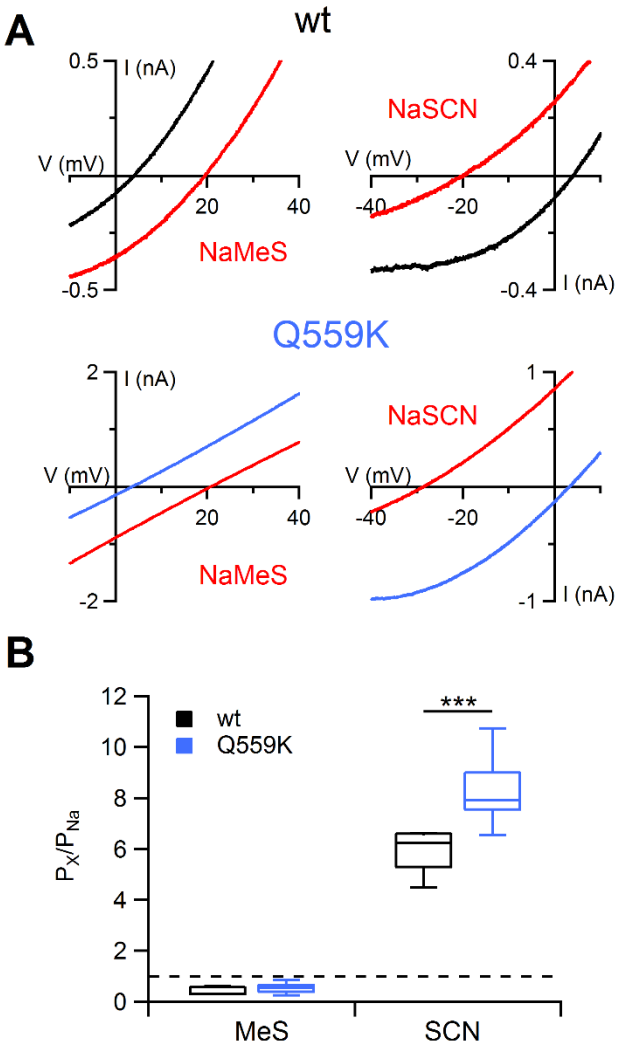

Figure 4. Anion and cation selectivity of TMEM16F-mediated current in whole-cell recordings. (A) Representative whole-cell voltage-clamp recordings obtained from TMEM16F wt or Q559K mutant transfected cells with intracellular solution containing 100 µM (wt) or 300 µM Ca^{2+} (mutant). Each cell was exposed to a control solution containing 140 mM NaCl (black/blue traces) then to the indicated salt. IV relation was determined by a voltage ramp from -100 to +100 mV but only region around the reversal potential is shown. (B) Comparison of the permeability ratio between substituted ions and Na^+ (P_X/P_{Na}) in TMEM16F wt and Q559K channels calculated with Goldman-Hodgkin-Katz equation (n=5-24; ** p<0.01, *** p<0.001 unpaired t-test).

Ca^{2+} activation of the TMEM16F-induced current in excised patches

To further investigate the Ca^{2+}-dependent activation of TMEM16F-induced current, we performed experiments by using the patch-clamp technique in the excised inside-out configuration from HEK 293 cells expressing TMEM16F wt and Q559K mutant. In these experiments, we used a perfusion system that allows a fast change of solution in less than 10 ms (Pifferi et al., 2009). Fig. 5A shows currents activated by the exposure of the cytoplasmic side of the patch to 1 mM Ca^{2+} for 2 s at the holding potential of +50 mV. Ca^{2+}-activated currents showed two time-dependent characteristics. In contrast with the results obtained in whole cell recordings both TMEM16F wt and Q559K could be rapidly activated upon application of 1 mM Ca^{2+}. However, the TMEM16F Q559K current could not reach a steady state level in 2 s (see also later). Moreover, both TMEM16F wt and Q559K current underwent to an irreversible decrease in the current amplitude with time, a process that we define as rundown (Fig. 5A-B). To determine the time course of the of rundown, we repeatedly exposed the excised inside-out patches to 1 mM Ca^{2+} for 2 s every 15 s keeping them in the nominally 0 Ca^{2+} between the calcium applications. Subsequent exposures to Ca^{2+} produced currents of decreasing amplitudes (Fig. 5B). We measured the peak current after each calcium application and we calculated the ratio between the value obtained at various times after patch excision and the maximal current measured just after the patch excision. The rundown was fast in the first minute after patch excision and slowed down with time, and sometimes the current reached a stationary current level (Fig. 5C). After 2.5 min the TMEM16F wt current decreased to 7 ± 1 % (n=31) of the starting value, while in Q559K mutant the current was reduced only to 35 ± 1 % (n=97, U-test $p=1.3 * 10^{-10}$). This difference could be explained by the fact that run-down is Ca^{2+}-dependent and higher at saturating concentration (Ye et al., 2018) and Q559K has lower Ca^{2+}-sensitivity (see below). Most of the following experiments were performed after the rapid phase of rundown when the current reached an almost steady-state value.

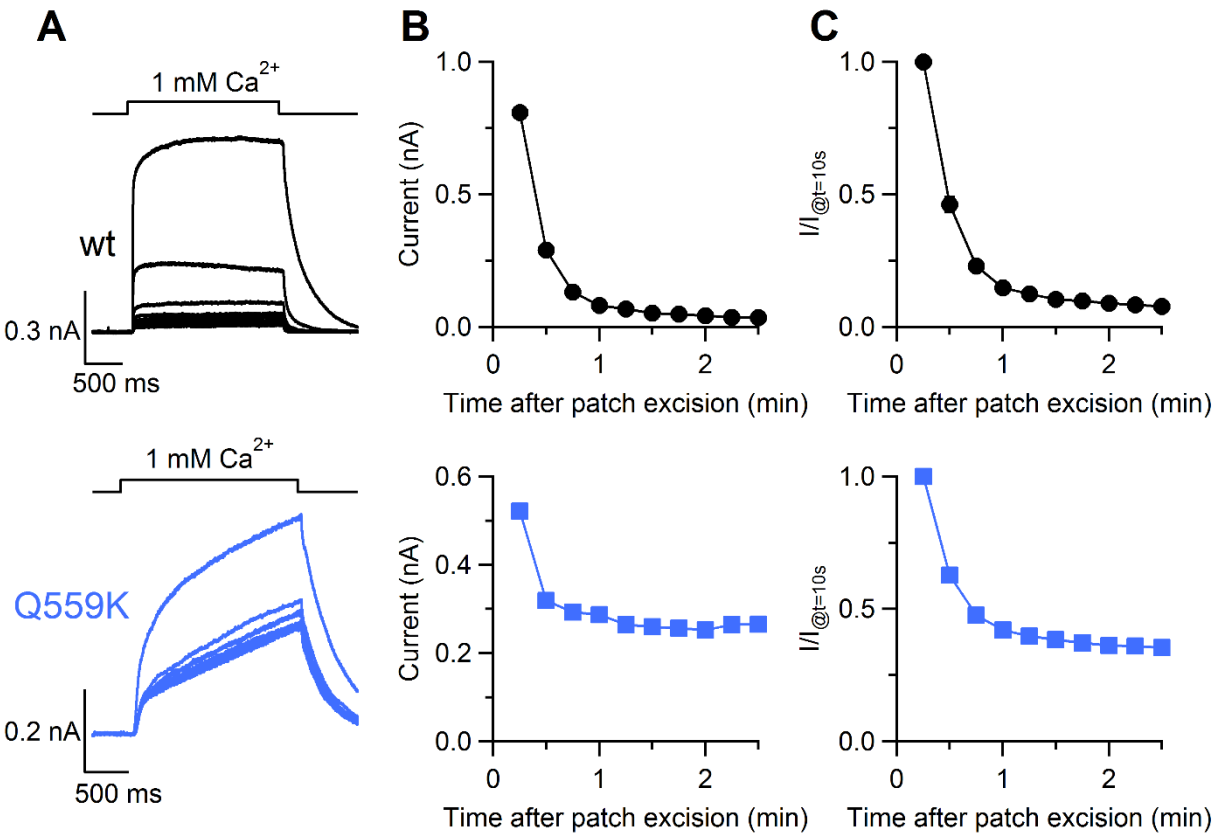

Figure 5. Rundown of TMEM16F-mediated current in excised inside-out membrane patches. (A) An inside-out excised membrane patch expressing TMEM16F wt or Q559K mutant was repeatedly stimulated with solution containing 1 mM Ca^{2+} at the time indicated in the upper traces. The holding potential was +50 mV. (B) The positive peak current from recordings in (A) was plotted against the time after patch excision. (C) Average ± sem of the ratios between the peak current at various times after patch excision and the maximal current measured at patch excision were plotted against the time after patch excision (n=31 for wt n=97 for Q559K).

Ca^{2+} sensitivity and current–voltage relation in excised patches

To measure the dependence of the TMEM16F-induced current on the intracellular Ca^{2+} concentration, dose–response relations were obtained in excised inside-out patches by activating currents with solutions containing various Ca^{2+} concentrations. Experiments were performed after the rapid phase of rundown when the current reached an almost steady-state value (Fig. 5). Figure 6 A illustrates the results of a representative dose-response experiment for TMEM16F wt and Q559K mutant channel at the holding potential of +60 mV. Normalized currents were plotted in Figure 6 B versus Ca^{2+} concentration and fitted by the Hill equation: $I/I_{max} = c^{nH} / (c^{nH} + K_{1/2}{}^{nH})$, where c is the Ca^{2+} concentration, $K_{1/2}$ the Ca^{2+} concentration producing half-maximal current activation, and n_H is the Hill coefficient. Q559K had a significant lower calcium sensitivity a $K_{1/2}$ of 201 ± 19 µM (n=7) significantly higher than 42 ± 6 µM obtained for TMEM16F wt channel

(n=7; p=1.1*10^{-4}, t-test). In addition, the Hill coefficient was significantly different between wt and Q599K suggesting a role in gating mechanism of this residue (n_H= 2.4 ± 0.3 for wt and 1.4 ± 0.2 for Q559K p=0.02 t-test).

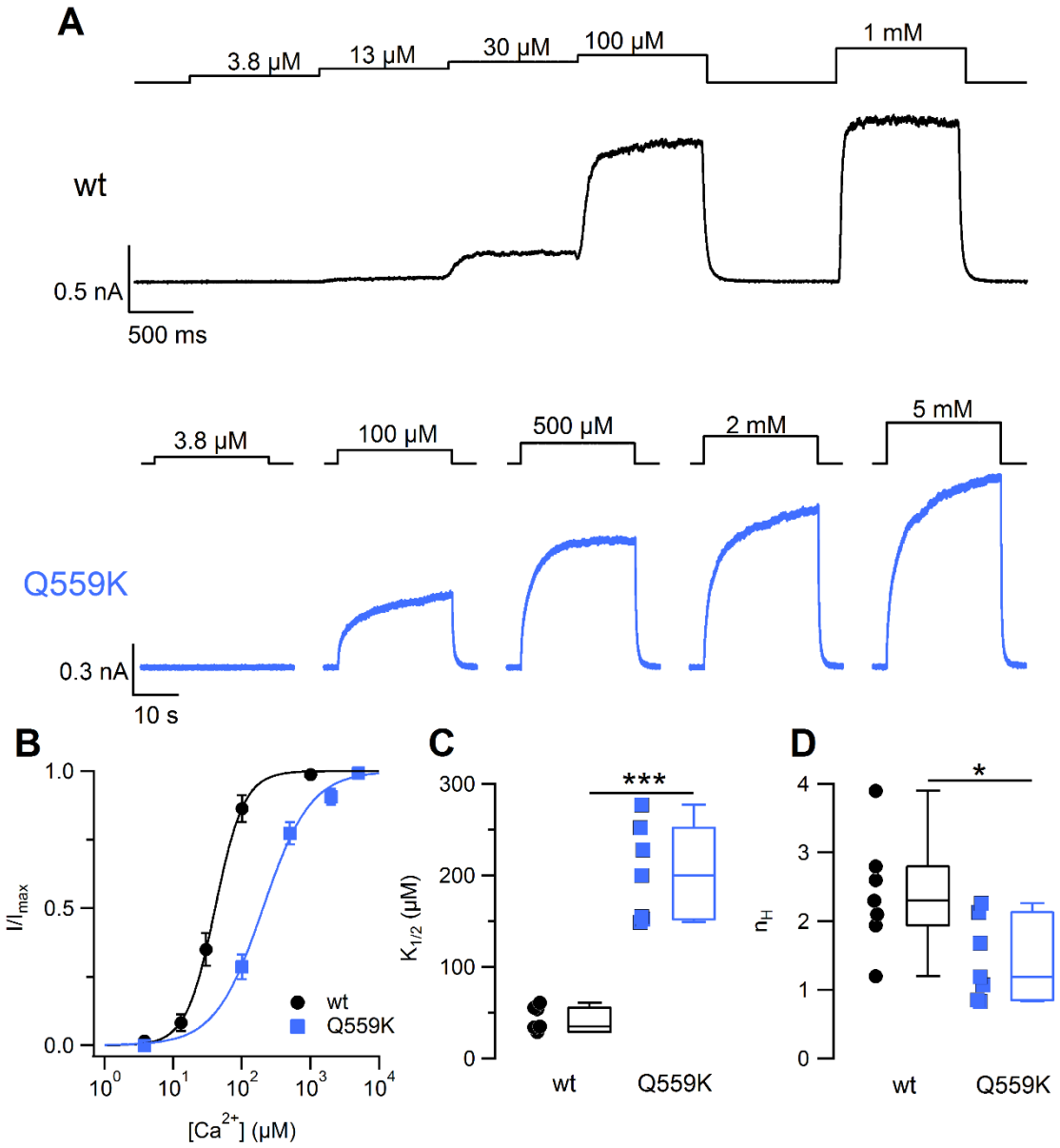

Figure 6. Ca^{2+} sensitivity of TMEM16F-mediated current in excised inside-out membrane patches. (A) An inside-out excised membrane patch expressing TMEM16F wt or Q559K mutant was stimulated with solutions containing different free Ca^{2+} concentration at the time indicated in the upper traces. The holding potential was +60 mV (B). Dose–response relations of activation by Ca^{2+} obtained by normalized currents fitted to the Hill equation. Comparison of $K_{1/2}$ (C) and n_H (D) obtained from TMEM16F wt and Q559K mutant channel (n=7; * p<0.05, ***p<0.001 unpaired t-test).

Furthermore, we measured the current–voltage relations in symmetrical NaCl solutions activating the current with 100 µM Ca^{2+}. We used a protocol with voltage steps of 500 ms duration given from a holding potential of -80 mV up to +100 mV in 10 mV intervals. As measured in whole cell recordings, both TMEM16F wt and Q559K mutant currents showed a strong outward rectification even at the high 100 µM Ca^{2+} concentration (Fig. 7 A-B). Only at voltages higher than +30 mV it was possible to record a current with a time-dependent kinetics and we fitted this relaxation at +100 mV with a single exponential function. The time constant for TMEM16F wt was 47 ± 11 ms (n=6), whereas a value of 456 ± 65 ms (n=6) was estimated for Q559K, showing a significantly slower kinetics in the mutant channel (p=0.001 t-test).

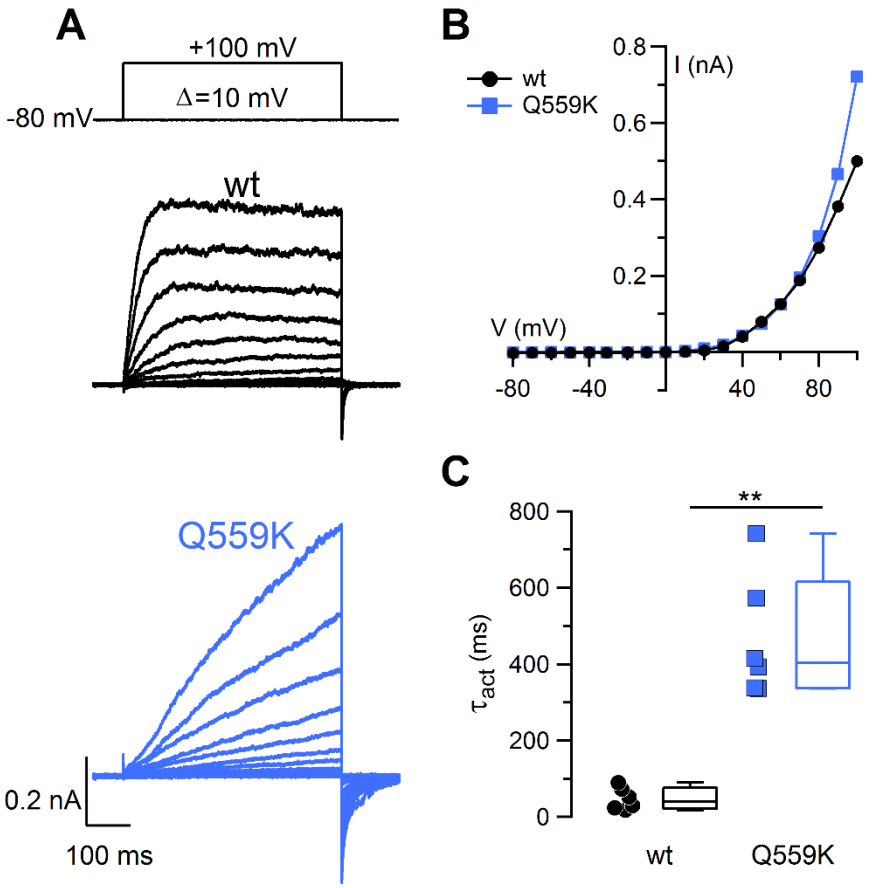

Figure 7 IV relation of TMEM16F-mediated current in excised inside-out membrane patches. (A) An inside-out excised membrane patch expressing mock, TMEM16F wt or Q559K mutant was exposed to solution containing 100 µM Ca^{2+} and stimulated with the voltage protocol as shown in the top part of the panel. Leakage currents measured in 0 Ca^{2+} were subtracted (B). I-V relations measured at the end of the voltage steps from the patches shown at the A. (C) Comparison of time constant of activation at +100 mV for TMEM16F wt and Q559K mutant channel (n=6; ** p<0.01, unpaired t-test).

Ionic selectivity in inside-out excised patches

To investigate the ionic selectivity of TMEM16F-mediated current observed in inside-out patches we used the dilution method as performed for whole-cell recordings (Barry, 2006). We activated the current with 100 µM Ca^{2+} for TMEM16F wt or with 1 mM Ca^{2+} for Q559K mutant. The NaCl concentration in bath solution was changed from 280 mM to 14 mM and the reversal potential was determined by using voltage ramps from +100 to -80 mV (Fig. 8 A-C). Reduction of NaCl in the intracellular solution caused a positive shift of the reversal potential in TMEM16F wt mediated current, whereas in Q559K we observed negative shift. Relative permeability ratios between Na^+ and Cl^- (P_{Na} /P_{Cl}) calculated with the Goldman–Hodgkin–Katz equation were 3.6 ± 0.1 (n=19) for wt channel and 0.71 ± 0.03 (n=18) for Q559K mutant ($p=1.15*10^{-15}$ t-test). The data show that the TMEM16F wt channel recorded in inside-out excised patches was relatively poorly selective but was more permeable to Na than to Cl^-, whereas in the mutant Q559K Cl^- was slightly more permeant than Na^+ (Fig. 8 D).

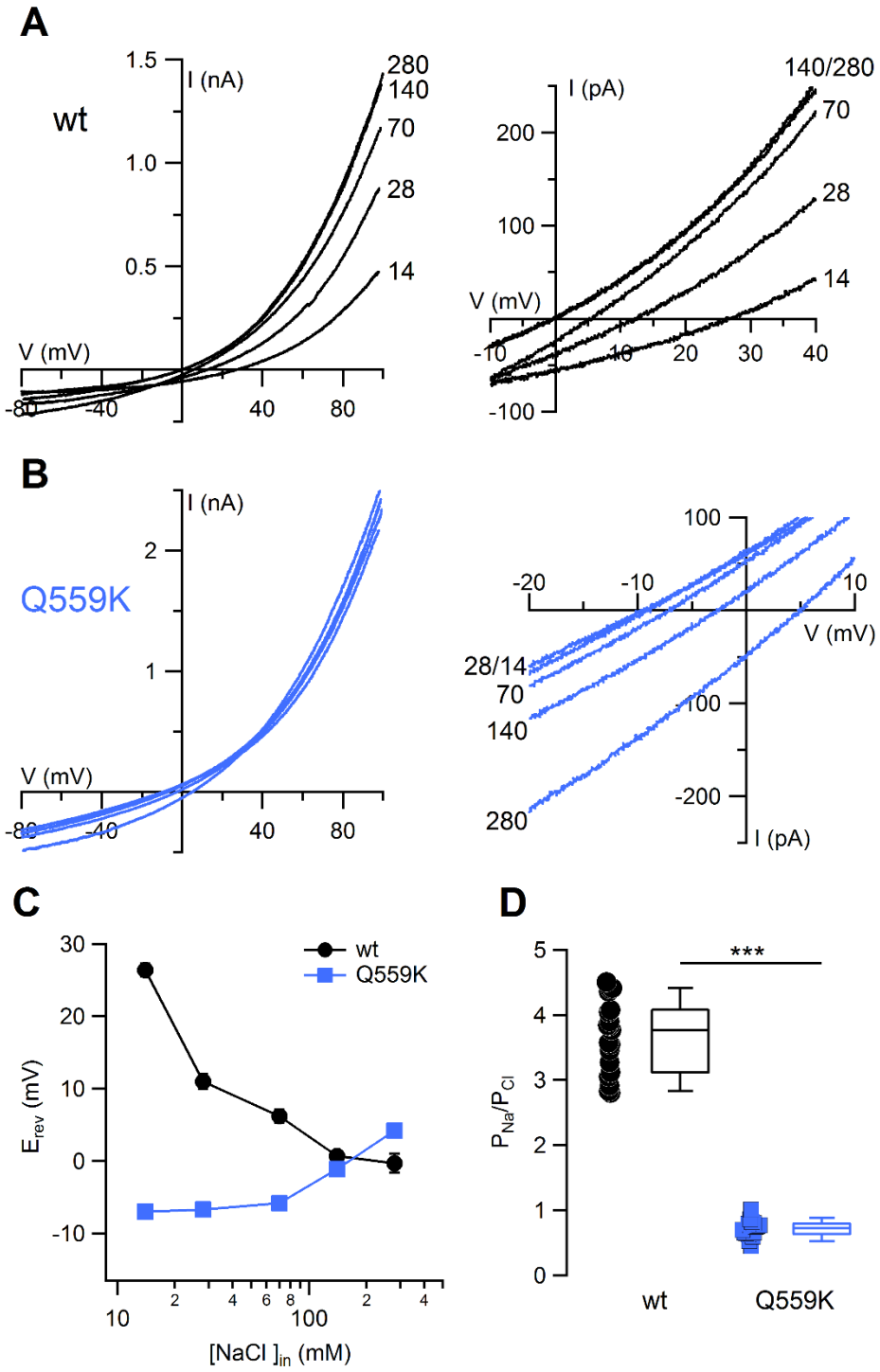

Figure 8 Ion selectivity of TMEM16F-mediated current in excised inside-out membrane patches. An inside-out patch expressing TMEM16F wt (A) or Q559K mutant (B) was exposed to different cytoplasmatic [NaCl] and the IV relation was determined by a voltage ramp from -80 to +100 mV. The current was activated by 100 µM $CaCl_2$ for wt and 1 mM for Q559K mutant. Leakage currents measured in 0 Ca^{2+} were subtracted. On the right panels the expanded graph around the reversal potential. (C) Average E_{rev} corrected for liquid junction potential was plotted versus $[NaCl]_i$ for TMEM16F wt or Q559K mutant (n = 9-19). (D) Comparison of the permeability ratio between Na^+ and Cl^- (P_{Na}/P_{Cl}) in TMEM16F wt and Q559K channels calculated with Goldman-Hodgkin-Katz equation from recordings with 14 mM $[NaCl]_i$ (n=18-19; *** $p<0.001$, unpaired t-test).

In order to determine the anion selectivity of TMEM16F-mediated current, we replaced NaCl in the bathing solution with Na salts of different anions and measured the shift in reversal potential by the same protocol used in the previous experiments (Fig. 9 AB). We calculated relative permeability ratios between different anions and Na^+ (P_X /P_{Na}) with the Goldman–Hodgkin–Katz equation taking also in account the Na^+ permeability measured with the dilution method (Fig. 8). Both TMEM16F wt and Q559K mutant channels were more permeable to some bigger anions than Cl^- but less permeable to MeS and Gluconate (Fig. 9 C). Relative permeability ratios were SCN (3.2 vs 9.1 wt vs Q559K)> I (1.47 vs 4.36)> NO_3 (1.25 vs 3.9) >Br (0.63 vs 2.39)> MeS (0.21 vs 0.58)> Gluconate (0.08 vs 0.53). TMEM16F wt and Q559K mutant channels showed the same permeability sequence even if Q559K had a higher permeability to all anions tested with respect to wt channel (at least $p<0.01$ t-test or U-test).

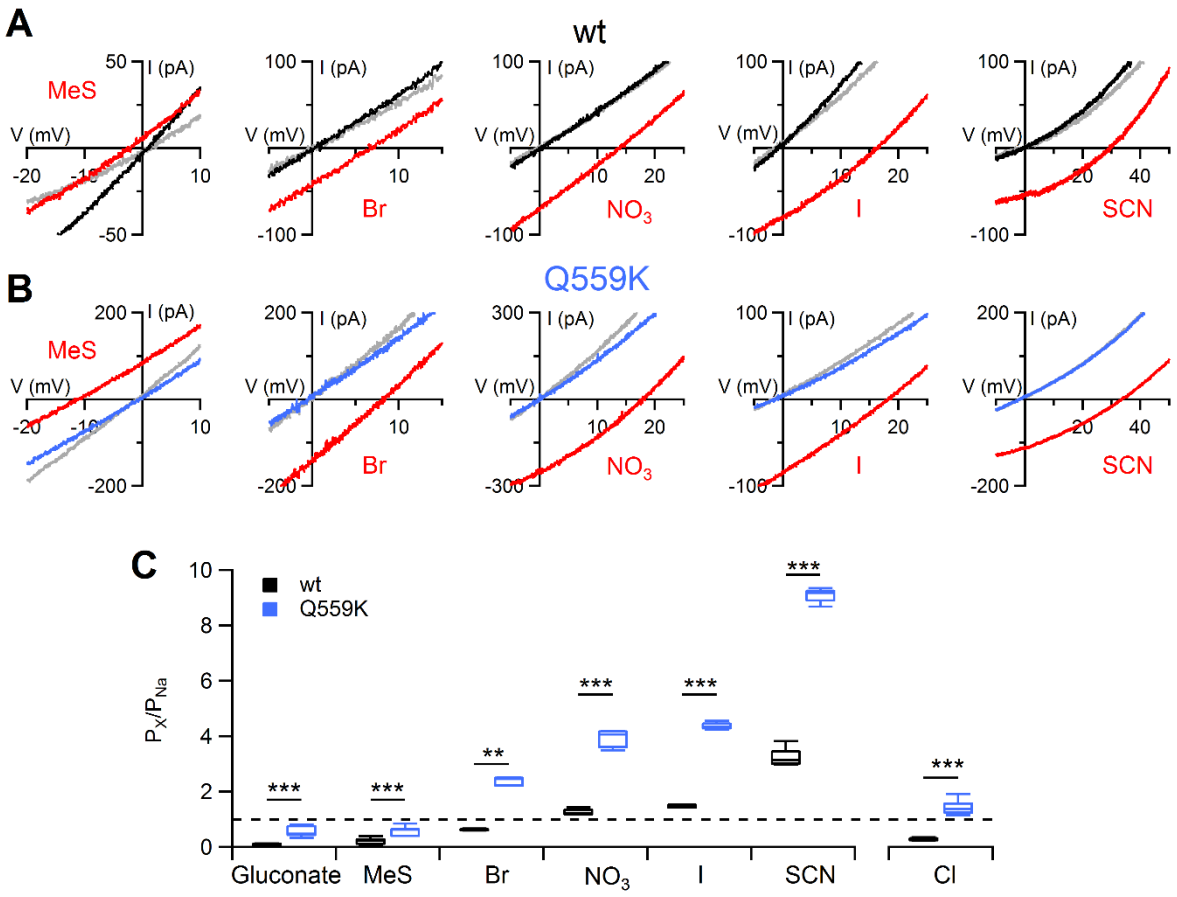

Figure 9 Anion selectivity of TMEM16F-mediated current in excised inside-out membrane patches. An inside-out patch expressing TMEM16F wt (A) or Q559K mutant (B) the indicated mutants was exposed to bath solutions containing 140 mM NaCl (black/blue traces) or the Na salt of other anions, as indicated. The gray traces represent the wash out with NaCl. IV relation was determined by a voltage ramp from -80 to +100 mV but only region around the reversal potential is shown. The current was activated by 1 mM $CaCl_2$. Leakage currents measured in 0 Ca^{2+} were subtracted. (C) Comparison of the permeability ratio between the between substituted anions and Na^+ (P_X/P_{Cl}) in TMEM16F wt and Q559K channels calculated with Goldman-Hodgkin-Katz equation (n=5-19; ** p<0.01, * ** p<0.001, unpaired t-test or U-test).

Finally, we determined the cation selectivity of TMEM16F-mediated current performing experiments in symmetrical NaMeS solution, replacing NaMes in the bathing solution with MeS salts of different cations and measuring the shift in reversal potential. By using Goldman–Hodgkin–Katz equation, we found that in TMEM16F wt channel K^+ was slightly more permeant than Na^+ (1.38 ± 0.04, n=7) , while both NMDG and TEA were less permeant (0.55 ± 0.01 for $NMDG^+$ and 0.519 ± 0.008 for TEA^+, n=5). In contrast, in Q559K mutant both K^+ and $NMDG^+$ are more permeant than Na^+ (1.93 ± 0.03 for K^+ and 1.29 ± 0.03 for $NMDG^+$, n=5-6) whereas TEA^+ did not have a significantly different permeability than Na^+ (0.98 ±0.02 n=5, p=0.35 one sample t-test).

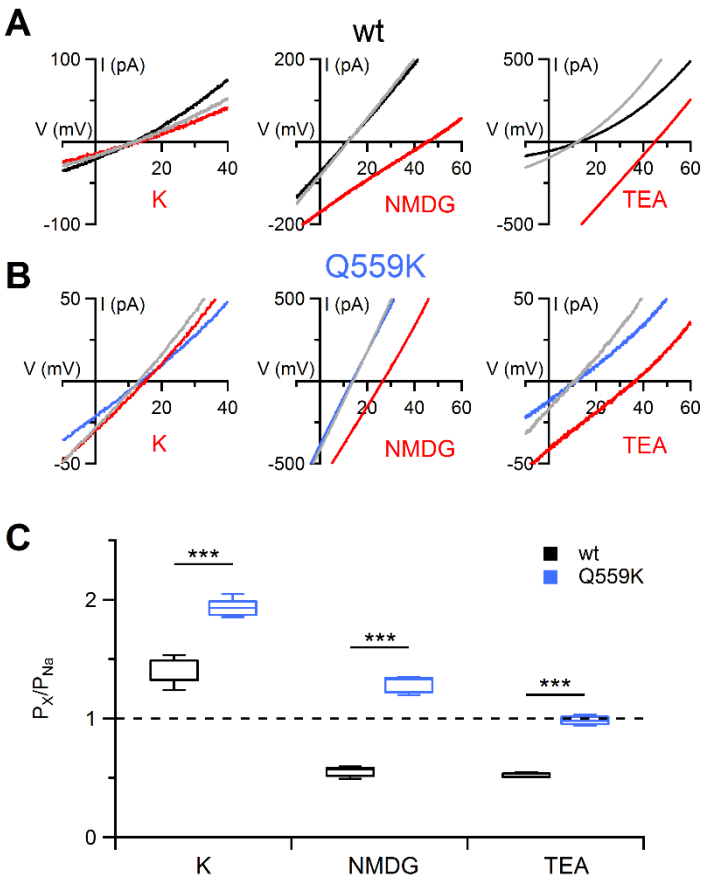

Figure 10 Cation selectivity of TMEM16F-mediated current in excised inside-out membrane patches. An inside-out patch expressing TMEM16F wt (A) or Q559K mutant (B) was exposed to bath solutions containing 140 mM NaMeS (black/blue traces) or the MeS salt of other cations, as indicated. The gray traces represent the wash out with NaMeS. IV relation was determined by a voltage ramp from -80 to +100 mV but only region around the reversal potential is shown. The current was activated by 100 µM $CaCl_2$ for wt and 1 mM for Q559K mutant. Leakage currents measured in 0 Ca^{2+} were subtracted. (C) Comparison of the permeability ratio between the between substituted cations and Na^+ (P_X/P_{Cl}) in TMEM16F wt and Q559K channels calculated with Goldman-Hodgkin-Katz equation (n=5-7; *** p<0.001, unpaired t-test).

References

Baig, A.A., Haining, E.J., Geuss, E., Beck, S., Swieringa, F., Wanitchakool, P., Schuhmann, M.K., Stegner, D., Kunzelmann, K., Kleinschnitz, C., et al. (2016). TMEM16F-Mediated Platelet Membrane Phospholipid Scrambling Is Critical for Hemostasis and Thrombosis but not Thromboinflammation in Mice-Brief Report. Arterioscler. Thromb. Vasc. Biol. *36*, 2152–2157.

Barry, P.H. (2006). The reliability of relative anion-cation permeabilities deduced from reversal (dilution) potential measurements in ion channel studies. Cell Biochem. Biophys. *46*, 143–154.

Brooks, M.B., Catalfamo, J.L., MacNguyen, R., Tim, D., Fancher, S., and McCardle, J.A. (2015). A TMEM16F point mutation causes an absence of canine platelet TMEM16F and ineffective activation and death-induced phospholipid scrambling. J. Thromb. Haemost. JTH *13*, 2240–2252.

Bulley, S., Neeb, Z.P., Burris, S.K., Bannister, J.P., Thomas-Gatewood, C.M., Jangsangthong, W., and Jaggar, J.H. (2012). TMEM16A/ANO1 channels contribute to the myogenic response in cerebral arteries. Circ. Res. *111*, 1027–1036.

Caputo, A., Caci, E., Ferrera, L., Pedemonte, N., Barsanti, C., Sondo, E., Pfeffer, U., Ravazzolo, R., Zegarra-Moran, O., and Galietta, L.J.V. (2008). TMEM16A, a membrane protein associated with calcium-dependent chloride channel activity. Science *322*, 590–594.

Coleman, J.A., Quazi, F., and Molday, R.S. (2013). Mammalian P4-ATPases and ABC transporters and their role in phospholipid transport. Biochim. Biophys. Acta *1831*, 555–574.

Danahay, H., Atherton, H., Jones, G., Bridges, R.J., and Poll, C.T. (2002). Interleukin-13 induces a hypersecretory ion transport phenotype in human bronchial epithelial cells. Am. J. Physiol. Lung Cell. Mol. Physiol. *282*, L226-236.

Dang, S., Feng, S., Tien, J., Peters, C.J., Bulkley, D., Lolicato, M., Zhao, J., Zuberbühler, K., Ye, W., Qi, L., et al. (2017). Cryo-EM structures of the TMEM16A calcium-activated chloride channel. Nature *552*, 426–429.

Davis, A.J., Forrest, A.S., Jepps, T.A., Valencik, M.L., Wiwchar, M., Singer, C.A., Sones, W.R., Greenwood, I.A., and Leblanc, N. (2010). Expression profile and protein translation of TMEM16A in murine smooth muscle. Am. J. Physiol. Cell Physiol. *299*, C948-959.

Davis, A.J., Shi, J., Pritchard, H.A.T., Chadha, P.S., Leblanc, N., Vasilikostas, G., Yao, Z., Verkman, A.S., Albert, A.P., and Greenwood, I.A. (2013). Potent vasorelaxant activity of the TMEM16A inhibitor T16A(inh) -A01. Br. J. Pharmacol. *168*, 773–784.

Ehlen, H.W.A., Chinenkova, M., Moser, M., Munter, H.-M., Krause, Y., Gross, S., Brachvogel, B., Wuelling, M., Kornak, U., and Vortkamp, A. (2013). Inactivation of anoctamin-6/Tmem16f, a regulator of phosphatidylserine scrambling in osteoblasts, leads to decreased mineral deposition in skeletal tissues. J. Bone Miner. Res. Off. J. Am. Soc. Bone Miner. Res. *28*, 246–259.

Galietta, L.J.V., Pagesy, P., Folli, C., Caci, E., Romio, L., Costes, B., Nicolis, E., Cabrini, G., Goossens, M., Ravazzolo, R., et al. (2002). IL-4 is a potent modulator of ion transport in the human bronchial epithelium in vitro. J. Immunol. Baltim. Md 1950 *168*, 839–845.

Grubb, S., Poulsen, K.A., Juul, C.A., Kyed, T., Klausen, T.K., Larsen, E.H., and Hoffmann, E.K. (2013). TMEM16F (Anoctamin 6), an anion channel of delayed Ca(2+) activation. J. Gen. Physiol. *141*, 585–600.

Hankins, H.M., Baldridge, R.D., Xu, P., and Graham, T.R. (2015). Role of flippases, scramblases and transfer proteins in phosphatidylserine subcellular distribution. Traffic Cph. Den. *16*, 35–47.

Henkel, B., Drose, D.R., Ackels, T., Oberland, S., Spehr, M., and Neuhaus, E.M. (2015). Co-expression of anoctamins in cilia of olfactory sensory neurons. Chem. Senses *40*, 73–87.

Huang, W.C., Xiao, S., Huang, F., Harfe, B.D., Jan, Y.N., and Jan, L.Y. (2012). Calcium-activated chloride channels (CaCCs) regulate action potential and synaptic response in hippocampal neurons. Neuron *74*, 179–192.

Kmit, A., van Kruchten, R., Ousingsawat, J., Mattheij, N.J.A., Senden-Gijsbers, B., Heemskerk, J.W.M., Schreiber, R., Bevers, E.M., and Kunzelmann, K. (2013). Calcium-activated and apoptotic phospholipid scrambling induced by Ano6 can occur independently of Ano6 ion currents. Cell Death Dis. *4*, e611.

van Kruchten, R., Mattheij, N.J.A., Saunders, C., Feijge, M.A.H., Swieringa, F., Wolfs, J.L.N., Collins, P.W., Heemskerk, J.W.M., and Bevers, E.M. (2013). Both TMEM16F-dependent and TMEM16F-independent pathways contribute to phosphatidylserine exposure in platelet apoptosis and platelet activation. Blood *121*, 1850–1857.

Manoury, B., Tamuleviciute, A., and Tammaro, P. (2010). TMEM16A/anoctamin 1 protein mediates calcium-activated chloride currents in pulmonary arterial smooth muscle cells. J. Physiol. *588*, 2305–2314.

Martins, J.R., Faria, D., Kongsuphol, P., Reisch, B., Schreiber, R., and Kunzelmann, K. (2011). Anoctamin 6 is an essential component of the outwardly rectifying chloride channel. Proc. Natl. Acad. Sci. U. S. A. *108*, 18168–18172.

van Meer, G. (2011). Dynamic transbilayer lipid asymmetry. Cold Spring Harb. Perspect. Biol. *3*.

Ousingsawat, J., Wanitchakool, P., Kmit, A., Romao, A.M., Jantarajit, W., Schreiber, R., and Kunzelmann, K. (2015). Anoctamin 6 mediates effects essential for innate immunity downstream of P2X7 receptors in macrophages. Nat. Commun. *6*, 6245.

Paulino, C., Kalienkova, V., Lam, A.K.M., Neldner, Y., and Dutzler, R. (2017). Activation mechanism of the calcium-activated chloride channel TMEM16A revealed by cryo-EM. Nature *552*, 421–425.

Pifferi, S., Dibattista, M., and Menini, A. (2009). TMEM16B induces chloride currents activated by calcium in mammalian cells. Pflüg. Arch. Eur. J. Physiol. *458*, 1023–1038.

Pomorski, T., and Menon, A.K. (2006). Lipid flippases and their biological functions. Cell. Mol. Life Sci. CMLS *63*, 2908–2921.

Rasche, S., Toetter, B., Adler, J., Tschapek, A., Doerner, J.F., Kurtenbach, S., Hatt, H., Meyer, H., Warscheid, B., and Neuhaus, E.M. (2010). Tmem16b is specifically expressed in the cilia of olfactory sensory neurons. Chem. Senses *35*, 239–245.

Schenk, L.K., Schulze, U., Henke, S., Weide, T., and Pavenstädt, H. (2016). TMEM16F Regulates Baseline Phosphatidylserine Exposure and Cell Viability in Human Embryonic Kidney Cells. Cell. Physiol. Biochem. Int. J. Exp. Cell. Physiol. Biochem. Pharmacol. *38*, 2452–2463.

Schreiber, R., Uliyakina, I., Kongsuphol, P., Warth, R., Mirza, M., Martins, J.R., and Kunzelmann, K. (2010). Expression and function of epithelial anoctamins. J. Biol. Chem. *285*, 7838–7845.

Schroeder, B.C., Cheng, T., Jan, Y.N., and Jan, L.Y. (2008). Expression cloning of TMEM16A as a calcium-activated chloride channel subunit. Cell *134*, 1019–1029.

Scudieri, P., Caci, E., Venturini, A., Sondo, E., Pianigiani, G., Marchetti, C., Ravazzolo, R., Pagani, F., and Galietta, L.J.V. (2015). Ion channel and lipid scramblase activity associated with expression of TMEM16F/ANO6 isoforms. J. Physiol. *593*, 3829–3848.

Shimizu, T., Iehara, T., Sato, K., Fujii, T., Sakai, H., and Okada, Y. (2013). TMEM16F is a component of a Ca2+-activated Cl- channel but not a volume-sensitive outwardly rectifying Cl- channel. Am. J. Physiol. Cell Physiol. *304*, C748-759.

Stephan, A.B., Shum, E.Y., Hirsh, S., Cygnar, K.D., Reisert, J., and Zhao, H. (2009). ANO2 is the cilial calcium-activated chloride channel that may mediate olfactory amplification. Proc. Natl. Acad. Sci. U. S. A. *106*, 11776–11781.

Stöhr, H., Heisig, J.B., Benz, P.M., Schöberl, S., Milenkovic, V.M., Strauss, O., Aartsen, W.M., Wijnholds, J., Weber, B.H.F., and Schulz, H.L. (2009). TMEM16B, a novel protein with calcium-dependent chloride channel activity, associates with a presynaptic protein complex in photoreceptor terminals. J. Neurosci. Off. J. Soc. Neurosci. *29*, 6809–6818.

Szteyn, K., Schmid, E., Nurbaeva, M.K., Yang, W., Münzer, P., Kunzelmann, K., Lang, F., and Shumilina, E. (2012). Expression and functional significance of the Ca(2+)-activated Cl(-) channel ANO6 in dendritic cells. Cell. Physiol. Biochem. Int. J. Exp. Cell. Physiol. Biochem. Pharmacol. *30*, 1319–1332.

Thomas-Gatewood, C., Neeb, Z.P., Bulley, S., Adebiyi, A., Bannister, J.P., Leo, M.D., and Jaggar, J.H. (2011). TMEM16A channels generate Ca^{2+}-activated Cl^- currents in cerebral artery smooth muscle cells. Am. J. Physiol. Heart Circ. Physiol. *301*, H1819-1827.

Yang, H., Kim, A., David, T., Palmer, D., Jin, T., Tien, J., Huang, F., Cheng, T., Coughlin, S.R., Jan, Y.N., et al. (2012). TMEM16F forms a Ca2+-activated cation channel required for lipid scrambling in platelets during blood coagulation. Cell *151*, 111–122.

Yang, Y.D., Cho, H., Koo, J.Y., Tak, M.H., Cho, Y., Shim, W.-S., Park, S.P., Lee, J., Lee, B., Kim, B.-M., et al. (2008). TMEM16A confers receptor-activated calcium-dependent chloride conductance. Nature *455*, 1210–1215.

Ye, W., Han, T.W., Nassar, L.M., Zubia, M., Jan, Y.N., and Jan, L.Y. (2018). Phosphatidylinositol-(4, 5)-bisphosphate regulates calcium gating of small-conductance cation channel TMEM16F.. Proc. Natl. Acad. Sci. U. S. A. *115*, E1667–E1674.

Yu, K., Whitlock, J.M., Lee, K., Ortlund, E.A., Cui, Y.Y., and Hartzell, H.C. (2015). Identification of a lipid scrambling domain in ANO6/TMEM16F. ELife *4*, e06901.

5. Discussion

TMEM16F ion selectivity is a matter of discussion in the literature and the data are diverse and often in contrast. Indeed, studies describing TMEM16F ion permeability report results which frequently lead to conflicting conclusions. For example, we noticed that experiments in studies reporting that TMEM16F is anion selective were performed only in the whole-cell configuration (Grubb et al., 2013; Scudieri et al., 2015; Shimizu et al., 2013; Szteyn et al., 2012), whereas results showing an higher permeability for cations were performed in the excised inside-out configuration (Yang et al., 2012). Thus, discrepancies in the results might be partially due to different technical approaches used in performing the experiment, such as different solutions or recording configurations.

In order to contribute to the clarification of the controversy, we decided to perform a complete and extended study of TMEM16F selectivity both in whole-cell and inside-out configurations using the same ion solutions, in order to compare the results. Our findings revealed substantial differences between the two configurations.

First of all, the current activation occurs with a different temporal scale. In the whole-cell configuration the complete activation of the current takes up to 4 minutes after membrane breaking. On the other hand, in inside-out the current is activated in few ms after the calcium application.

We also found a significant difference in terms of ion permeability. Our results showed that in whole-cell, TMEM16F is weakly selective for anions, with $P_{Na}/P_{Cl} \approx 0.5$. The replacing Cl^- with SCN^- and MeS^- induced slight shifts of reversal potentials, which indicate an anion selectivity. On the other hand, the recordings performed in inside-out showed that TMEM16F has a higher permeability for cations, with $P_{Na}/P_{Cl} \approx 3.5$.

We found that Q559K mutation affects Ca^{2+} sensitivity: the $K_{1/2}$ is almost 5-folds higher than the value obationed from wild type channel. Q559K mutant showed also a reduction of Hill coefficient, which might indicate an alteration of the gating mechanism. The low Ca^{2+} sensitivity we found could explain why Scudieri et al. (2015) did not find any current recording the Q559K mutant in whole-cell configuration (Scudieri et al.,

2015). Indeed, in their recordings they used 20 µM of intracellular Ca^{2+}, which is not sufficient to activate the mutated channel according to our data.

Thus, we found that TMEM16F ion selectivity is different depending on the electrophysiological approach used to analyze it and we speculate that this difference might be due to a cellular mechanism present in the cytoplasm, which plays a role in controlling TMEM16F channel activation and ion selectivity and is missing in excised patches.

This cellular mechanism is unknown, but based on data in the literature we can speculate about some possibilities. Lin et al. (2018), showed that TMEM16F activation and deactivation in whole-cell are affected by the cytoskeleton. In particular, they found that molecules stabilizing actin filaments prevented current activation, while molecules interfering with actin polymerization accelerated TMEM16F activation. Moreover, they found that ATP delayed the activation and prevented the inactivation of the current (Lin et al., 2018). Kim et al. (2015), found that the inhibitors of serotonin reuptake, such as fluoxetine and paroxetine, facilitated TMEM16F current activation in whole-cell recordings. Interestingly, the same drugs reduced TMEM16F current amplitude if perfused on excised patches, suggesting that the inhibitor probably required another component which is missing in excised patches (Kim et al., 2015). Another candidate for controlling TMEM16F properties could be Calmodulin. Possible Calmodulin-TMEM16F interaction has not been investigated yet and it is still unknown if Calmodulin controls TMEM16F. On the other hand, has been showed that Calmodulin physically interact with TMEM16A in Ca^{2+}-dependent manner and is responsible for changes in anion permeability at high intracellular Ca^{2+} concentration. In addition, the exposure of excised patches to recombinant Calmodulin increased the permeability ratio P_{HCO_3}/P_{Cl}. (Jung et al., 2013).

According with these data, additional experiments are necessary to better characterize these interesting aspects of TMEM16F. Proteomic approaches could be used to test possible interactors of TMEM16F able to regulate its biophysical properties. A better description of the endogenous TMEM16F current properties could be important to extend the knowledge that we have about this channel and its ion selectivity. Analysis of TMEM16F in artificial bilayers may be useful in order to avoid any

disturb due to other channels expressed in cells. Furthermore, new mutants of TMEM16F could help in understanding which residues play an important role in controlling ion selectivity.

6. References

Adomaviciene, A., Smith, K.J., Garnett, H., and Tammaro, P. (2013). Putative pore-loops of TMEM16/anoctamin channels affect channel density in cell membranes. J. Physiol. *591*, 3487–3505.

Amjad, A., Hernandez-Clavijo, A., Pifferi, S., Maurya, D.K., Boccaccio, A., Franzot, J., Rock, J., and Menini, A. (2015). Conditional knockout of TMEM16A/anoctamin1 abolishes the calcium-activated chloride current in mouse vomeronasal sensory neurons. J. Gen. Physiol. *145*, 285–301.

Ayoub, C., Wasylyk, C., Li, Y., Thomas, E., Marisa, L., Robé, A., Roux, M., Abecassis, J., de Reyniès, A., and Wasylyk, B. (2010). ANO1 amplification and expression in HNSCC with a high propensity for future distant metastasis and its functions in HNSCC cell lines. Br. J. Cancer *103*, 715–726.

Baig, A.A., Haining, E.J., Geuss, E., Beck, S., Swieringa, F., Wanitchakool, P., Schuhmann, M.K., Stegner, D., Kunzelmann, K., Kleinschnitz, C., et al. (2016). TMEM16F-Mediated Platelet Membrane Phospholipid Scrambling Is Critical for Hemostasis and Thrombosis but not Thromboinflammation in Mice-Brief Report. Arterioscler. Thromb. Vasc. Biol. *36*, 2152–2157.

Betto, G., Cherian, O.L., Pifferi, S., Cenedese, V., Boccaccio, A., and Menini, A. (2014). Interactions between permeation and gating in the TMEM16B/anoctamin2 calcium-activated chloride channel. J. Gen. Physiol. *143*, 703–718.

Bevers, E.M., and Williamson, P.L. (2010). Phospholipid scramblase: an update. FEBS Lett. *584*, 2724–2730.

Bill, A., Gutierrez, A., Kulkarni, S., Kemp, C., Bonenfant, D., Voshol, H., Duvvuri, U., and Gaither, L.A. (2015). ANO1/TMEM16A interacts with EGFR and correlates with sensitivity to EGFR-targeting therapy in head and neck cancer. Oncotarget *6*, 9173–9188.

Billig, G.M., Pál, B., Fidzinski, P., and Jentsch, T.J. (2011). Ca2+-activated Cl− currents are dispensable for olfaction. Nat. Neurosci. *14*, 763–769.

Britschgi, A., Bill, A., Brinkhaus, H., Rothwell, C., Clay, I., Duss, S., Rebhan, M., Raman, P., Guy, C.T., Wetzel, K., et al. (2013). Calcium-activated chloride channel ANO1 promotes breast cancer progression by activating EGFR and CAMK signaling. Proc. Natl. Acad. Sci. U. S. A. *110*, E1026-1034.

Brunner, J.D., Lim, N.K., Schenck, S., Duerst, A., and Dutzler, R. (2014). X-ray structure of a calcium-activated TMEM16 lipid scramblase. Nature *516*, 207–212.

Brunner, J.D., Schenck, S., and Dutzler, R. (2016). Structural basis for phospholipid scrambling in the TMEM16 family. Curr. Opin. Struct. Biol. *39*, 61–70.

Buchholz, B., Faria, D., Schley, G., Schreiber, R., Eckardt, K.-U., and Kunzelmann, K. (2014). Anoctamin 1 induces calcium-activated chloride secretion and proliferation of renal cyst-forming epithelial cells. Kidney Int. *85*, 1058–1067.

Bulley, S., Neeb, Z.P., Burris, S.K., Bannister, J.P., Thomas-Gatewood, C.M., Jangsangthong, W., and Jaggar, J.H. (2012). TMEM16A/ANO1 channels contribute to the myogenic response in cerebral arteries. Circ. Res. *111*, 1027–1036.

Caputo, A., Caci, E., Ferrera, L., Pedemonte, N., Barsanti, C., Sondo, E., Pfeffer, U., Ravazzolo, R., Zegarra-Moran, O., and Galietta, L.J.V. (2008). TMEM16A, a membrane protein associated with calcium-dependent chloride channel activity. Science *322*, 590–594.

Chen, Y., An, H., Li, T., Liu, Y., Gao, C., Guo, P., Zhang, H., and Zhan, Y. (2011). Direct or indirect regulation of calcium-activated chloride channel by calcium. J. Membr. Biol. *240*, 121–129.

Cho, H., Yang, Y.D., Lee, J., Lee, B., Kim, T., Jang, Y., Back, S.K., Na, H.S., Harfe, B.D., Wang, F., et al. (2012). The calcium-activated chloride channel anoctamin 1 acts as a heat sensor in nociceptive neurons. Nat. Neurosci. *15*, 1015–1021.

Coleman, J.A., Quazi, F., and Molday, R.S. (2013). Mammalian P4-ATPases and ABC transporters and their role in phospholipid transport. Biochim. Biophys. Acta *1831*, 555–574.

Danahay, H., Atherton, H., Jones, G., Bridges, R.J., and Poll, C.T. (2002). Interleukin-13 induces a hypersecretory ion transport phenotype in human bronchial epithelial cells. Am. J. Physiol. Lung Cell. Mol. Physiol. *282*, L226-236.

Dang, S., Feng, S., Tien, J., Peters, C.J., Bulkley, D., Lolicato, M., Zhao, J., Zuberbühler, K., Ye, W., Qi, L., et al. (2017). Cryo-EM structures of the TMEM16A calcium-activated chloride channel. Nature *552*, 426–429.

Dauner, K., Lissmann, J., Jeridi, S., Frings, S., and Möhrlen, F. (2012). Expression patterns of anoctamin 1 and anoctamin 2 chloride channels in the mammalian nose. Cell Tissue Res. *347*, 327–341.

Davis, A.J., Forrest, A.S., Jepps, T.A., Valencik, M.L., Wiwchar, M., Singer, C.A., Sones, W.R., Greenwood, I.A., and Leblanc, N. (2010). Expression profile and protein translation of TMEM16A in murine smooth muscle. Am. J. Physiol. Cell Physiol. *299*, C948-959.

Davis, A.J., Shi, J., Pritchard, H.A.T., Chadha, P.S., Leblanc, N., Vasilikostas, G., Yao, Z., Verkman, A.S., Albert, A.P., and Greenwood, I.A. (2013). Potent vasorelaxant activity of the TMEM16A inhibitor T16A(inh) -A01. Br. J. Pharmacol. *168*, 773–784.

De Jesús-Pérez, J.J., Cruz-Rangel, S., Espino-Saldaña, Á.E., Martínez-Torres, A., Qu, Z., Hartzell, H.C., Corral-Fernandez, N.E., Pérez-Cornejo, P., and Arreola, J. (2018). Phosphatidylinositol 4,5-bisphosphate, cholesterol, and fatty acids modulate the calcium-activated chloride channel TMEM16A (ANO1). Biochim. Biophys. Acta Mol. Cell Biol. Lipids *1863*, 299–312.

Di Zanni, E., Gradogna, A., Scholz-Starke, J., and Boccaccio, A. (2018). Gain of function of TMEM16E/ANO5 scrambling activity caused by a mutation associated with gnathodiaphyseal dysplasia. Cell. Mol. Life Sci. CMLS *75*, 1657–1670.

Dibattista, M., Amjad, A., Maurya, D.K., Sagheddu, C., Montani, G., Tirindelli, R., and Menini, A. (2012). Calcium-activated chloride channels in the apical region of mouse vomeronasal sensory neurons. J. Gen. Physiol. *140*, 3–15.

Dibattista, M., Pifferi, S., Boccaccio, A., Menini, A., and Reisert, J. (2017). The long tale of the calcium activated Cl- channels in olfactory transduction. Channels Austin Tex *11*, 399–414.

Dixit, R., Kemp, C., Kulich, S., Seethala, R., Chiosea, S., Ling, S., Ha, P.K., and Duvvuri, U. (2015). TMEM16A/ANO1 is differentially expressed in HPV-negative versus HPV-positive head and neck squamous cell carcinoma through promoter methylation. Sci. Rep. *5*, 16657.

Duvvuri, U., Shiwarski, D.J., Xiao, D., Bertrand, C., Huang, X., Edinger, R.S., Rock, J.R., Harfe, B.D., Henson, B.J., Kunzelmann, K., et al. (2012). TMEM16A induces MAPK and contributes directly to tumorigenesis and cancer progression. Cancer Res. *72*, 3270–3281.

Ehlen, H.W.A., Chinenkova, M., Moser, M., Munter, H.-M., Krause, Y., Gross, S., Brachvogel, B., Wuelling, M., Kornak, U., and Vortkamp, A. (2013). Inactivation of anoctamin-6/Tmem16f, a regulator of phosphatidylserine scrambling in osteoblasts, leads to decreased mineral deposition in skeletal tissues. J. Bone Miner. Res. Off. J. Am. Soc. Bone Miner. Res. *28*, 246–259.

Falzone, M.E., Malvezzi, M., Lee, B.-C., and Accardi, A. (2018). Known structures and unknown mechanisms of TMEM16 scramblases and channels. J. Gen. Physiol. *150*, 933–947.

Ferrera, L., Caputo, A., Ubby, I., Bussani, E., Zegarra-Moran, O., Ravazzolo, R., Pagani, F., and Galietta, L.J.V. (2009). Regulation of TMEM16A chloride channel properties by alternative splicing. J. Biol. Chem. *284*, 33360–33368.

Forrest, A.S., Joyce, T.C., Huebner, M.L., Ayon, R.J., Wiwchar, M., Joyce, J., Freitas, N., Davis, A.J., Ye, L., Duan, D.D., et al. (2012). Increased TMEM16A-encoded calcium-activated chloride channel activity is associated with pulmonary hypertension. Am. J. Physiol. Cell Physiol. *303*, C1229-1243.

Fujii, T., Sakata, A., Nishimura, S., Eto, K., and Nagata, S. (2015). TMEM16F is required for phosphatidylserine exposure and microparticle release in activated mouse platelets. Proc. Natl. Acad. Sci. U. S. A. *112*, 12800–12805.

Galietta, L.J.V., Pagesy, P., Folli, C., Caci, E., Romio, L., Costes, B., Nicolis, E., Cabrini, G., Goossens, M., Ravazzolo, R., et al. (2002). IL-4 is a potent modulator of ion transport in the human bronchial epithelium in vitro. J. Immunol. Baltim. Md 1950 *168*, 839–845.

Grubb, S., Poulsen, K.A., Juul, C.A., Kyed, T., Klausen, T.K., Larsen, E.H., and Hoffmann, E.K. (2013). TMEM16F (Anoctamin 6), an anion channel of delayed Ca(2+) activation. J. Gen. Physiol. *141*, 585–600.

Gyobu, S., Ishihara, K., Suzuki, J., Segawa, K., and Nagata, S. (2017). Characterization of the scrambling domain of the TMEM16 family. Proc. Natl. Acad. Sci. U. S. A. *114*, 6274–6279.

Ha, G.E., Lee, J., Kwak, H., Song, K., Kwon, J., Jung, S.-Y., Hong, J., Chang, G.-E., Hwang, E.M., Shin, H.-S., et al. (2016). The Ca2+-activated chloride channel anoctamin-2 mediates spike-frequency adaptation and regulates sensory transmission in thalamocortical neurons. Nat. Commun. *7*, 13791.

Hahn, Y., Kim, D.S., Pastan, I.H., and Lee, B. (2009). Anoctamin and transmembrane channel-like proteins are evolutionarily related. Int. J. Mol. Med. *24*, 51–55.

Hankins, H.M., Baldridge, R.D., Xu, P., and Graham, T.R. (2015). Role of flippases, scramblases and transfer proteins in phosphatidylserine subcellular distribution. Traffic Cph. Den. *16*, 35–47.

Henkel, B., Drose, D.R., Ackels, T., Oberland, S., Spehr, M., and Neuhaus, E.M. (2015). Co-expression of anoctamins in cilia of olfactory sensory neurons. Chem. Senses *40*, 73–87.

Hille, B., Dickson, E.J., Kruse, M., Vivas, O., and Suh, B.-C. (2015). Phosphoinositides regulate ion channels. Biochim. Biophys. Acta *1851*, 844–856.

Huang, F., Wang, X., Ostertag, E.M., Nuwal, T., Huang, B., Jan, Y.-N., Basbaum, A.I., and Jan, L.Y. (2013). TMEM16C facilitates Na(+)-activated K+ currents in rat sensory neurons and regulates pain processing. Nat. Neurosci. *16*, 1284–1290.

Huang, W.C., Xiao, S., Huang, F., Harfe, B.D., Jan, Y.N., and Jan, L.Y. (2012). Calcium-activated chloride channels (CaCCs) regulate action potential and synaptic response in hippocampal neurons. Neuron *74*, 179–192.

Jacobsen, K.S., Zeeberg, K., Sauter, D.R.P., Poulsen, K.A., Hoffmann, E.K., and Schwab, A. (2013). The role of TMEM16A (ANO1) and TMEM16F (ANO6) in cell migration. Pflugers Arch. *465*, 1753–1762.

Jia, L., Liu, W., Guan, L., Lu, M., and Wang, K. (2015). Inhibition of Calcium-Activated Chloride Channel ANO1/TMEM16A Suppresses Tumor Growth and Invasion in Human Lung Cancer. PloS One *10*, e0136584.

Jung, J., Nam, J.H., Park, H.W., Oh, U., Yoon, J.-H., and Lee, M.G. (2013). Dynamic modulation of ANO1/TMEM16A HCO3(-) permeability by Ca2+/calmodulin. Proc. Natl. Acad. Sci. U. S. A. *110*, 360–365.

Juul, C.A., Grubb, S., Poulsen, K.A., Kyed, T., Hashem, N., Lambert, I.H., Larsen, E.H., and Hoffmann, E.K. (2014). Anoctamin 6 differs from VRAC and VSOAC but is involved in apoptosis and supports volume regulation in the presence of Ca2+. Pflugers Arch. *466*, 1899–1910.

Kim, H.J., Jun, I., Yoon, J.S., Jung, J., Kim, Y.K., Kim, W.K., Kim, B.J., Song, J., Kim, S.J., Nam, J.H., et al. (2015). Selective serotonin reuptake inhibitors facilitate ANO6 (TMEM16F) current activation and phosphatidylserine exposure. Pflugers Arch. *467*, 2243–2256.

Kmit, A., van Kruchten, R., Ousingsawat, J., Mattheij, N.J.A., Senden-Gijsbers, B., Heemskerk, J.W.M., Schreiber, R., Bevers, E.M., and Kunzelmann, K. (2013). Calcium-activated and apoptotic phospholipid scrambling induced by Ano6 can occur independently of Ano6 ion currents. Cell Death Dis. *4*, e611.

van Kruchten, R., Mattheij, N.J.A., Saunders, C., Feijge, M.A.H., Swieringa, F., Wolfs, J.L.N., Collins, P.W., Heemskerk, J.W.M., and Bevers, E.M. (2013). Both TMEM16F-dependent and TMEM16F-independent pathways contribute to phosphatidylserine exposure in platelet apoptosis and platelet activation. Blood *121*, 1850–1857.

Kuruma, A., and Hartzell, H.C. (1999). Dynamics of calcium regulation of chloride currents in Xenopus oocytes. Am. J. Physiol. *276*, C161-175.

Lee, B.-C., Menon, A.K., and Accardi, A. (2016). The nhTMEM16 Scramblase Is Also a Nonselective Ion Channel. Biophys. J. *111*, 1919–1924.

Lee, B.-C., Khelashvili, G., Falzone, M., Menon, A.K., Weinstein, H., and Accardi, A. (2018). Gating mechanism of the extracellular entry to the lipid pathway in a TMEM16 scramblase. Nat. Commun. *9*, 3251.

Lin, H., Roh, J., Woo, J.H., Kim, S.J., and Nam, J.H. (2018). TMEM16F/ANO6, a Ca2+-activated anion channel, is negatively regulated by the actin cytoskeleton and intracellular MgATP. Biochem. Biophys. Res. Commun. *503*, 2348–2354.

Liu, B., Linley, J.E., Du, X., Zhang, X., Ooi, L., Zhang, H., and Gamper, N. (2010). The acute nociceptive signals induced by bradykinin in rat sensory neurons are mediated by inhibition of M-type K+ channels and activation of Ca2+-activated Cl- channels. J. Clin. Invest. *120*, 1240–1252.

Liu, J., Liu, Y., Ren, Y., Kang, L., and Zhang, L. (2014). Transmembrane protein with unknown function 16A overexpression promotes glioma formation through the nuclear factor-κB signaling pathway. Mol. Med. Rep. *9*, 1068–1074.

Liu, W., Lu, M., Liu, B., Huang, Y., and Wang, K. (2012). Inhibition of Ca(2+)-activated Cl(-) channel ANO1/TMEM16A expression suppresses tumor growth and invasiveness in human prostate carcinoma. Cancer Lett. *326*, 41–51.

Malvezzi, M., Chalat, M., Janjusevic, R., Picollo, A., Terashima, H., Menon, A.K., and Accardi, A. (2013). Ca2+-dependent phospholipid scrambling by a reconstituted TMEM16 ion channel. Nat. Commun. *4*, 2367.

Manoury, B., Tamuleviciute, A., and Tammaro, P. (2010). TMEM16A/anoctamin 1 protein mediates calcium-activated chloride currents in pulmonary arterial smooth muscle cells. J. Physiol. *588*, 2305–2314.

Martins, J.R., Faria, D., Kongsuphol, P., Reisch, B., Schreiber, R., and Kunzelmann, K. (2011). Anoctamin 6 is an essential component of the outwardly rectifying chloride channel. Proc. Natl. Acad. Sci. U. S. A. *108*, 18168–18172.

Maurya, D.K., and Menini, A. (2014). Developmental expression of the calcium-activated chloride channels TMEM16A and TMEM16B in the mouse olfactory epithelium. Dev. Neurobiol. *74*, 657–675.

van Meer, G. (2011). Dynamic transbilayer lipid asymmetry. Cold Spring Harb. Perspect. Biol. *3*.

Milenkovic, V.M., Brockmann, M., Stöhr, H., Weber, B.H., and Strauss, O. (2010). Evolution and functional divergence of the anoctamin family of membrane proteins. BMC Evol. Biol. *10*, 319.

Neureither, F., Stowasser, N., Frings, S., and Möhrlen, F. (2017). Tracking of unfamiliar odors is facilitated by signal amplification through anoctamin 2 chloride channels in mouse olfactory receptor neurons. Physiol. Rep. *5*.

Ni, Y.-L., Kuan, A.-S., and Chen, T.-Y. (2014). Activation and inhibition of TMEM16A calcium-activated chloride channels. PloS One *9*, e86734.

Ousingsawat, J., Wanitchakool, P., Schreiber, R., Wuelling, M., Vortkamp, A., and Kunzelmann, K. (2015a). Anoctamin-6 controls bone mineralization by activating the calcium transporter NCX1. J. Biol. Chem. *290*, 6270–6280.

Ousingsawat, J., Wanitchakool, P., Kmit, A., Romao, A.M., Jantarajit, W., Schreiber, R., and Kunzelmann, K. (2015b). Anoctamin 6 mediates effects essential for innate immunity downstream of P2X7 receptors in macrophages. Nat. Commun. *6*, 6245.

Paulino, C., Kalienkova, V., Lam, A.K.M., Neldner, Y., and Dutzler, R. (2017a). Activation mechanism of the calcium-activated chloride channel TMEM16A revealed by cryo-EM. Nature *552*, 421–425.

Paulino, C., Neldner, Y., Lam, A.K., Kalienkova, V., Brunner, J.D., Schenck, S., and Dutzler, R. (2017b). Structural basis for anion conduction in the calcium-activated chloride channel TMEM16A. ELife *6*.

Perez-Cornejo, P., De Santiago, J.A., and Arreola, J. (2004). Permeant anions control gating of calcium-dependent chloride channels. J. Membr. Biol. *198*, 125–133.

Peters, C.J., Gilchrist, J.M., Tien, J., Bethel, N.P., Qi, L., Chen, T., Wang, L., Jan, Y.N., Grabe, M., and Jan, L.Y. (2018). The Sixth Transmembrane Segment Is a Major Gating Component of the TMEM16A Calcium-Activated Chloride Channel. Neuron *97*, 1063-1077.e4.

Pietra, G., Dibattista, M., Menini, A., Reisert, J., and Boccaccio, A. (2016). The Ca2+-activated Cl- channel TMEM16B regulates action potential firing and axonal targeting in olfactory sensory neurons. J. Gen. Physiol. *148*, 293–311.

Pifferi, S., Dibattista, M., and Menini, A. (2009). TMEM16B induces chloride currents activated by calcium in mammalian cells. Pflüg. Arch. Eur. J. Physiol. *458*, 1023–1038.

Pomorski, T., and Menon, A.K. (2006). Lipid flippases and their biological functions. Cell. Mol. Life Sci. CMLS *63*, 2908–2921.

Ponissery Saidu, S., Stephan, A.B., Talaga, A.K., Zhao, H., and Reisert, J. (2013). Channel properties of the splicing isoforms of the olfactory calcium-activated chloride channel Anoctamin 2. J. Gen. Physiol. *141*, 691–703.

Rasche, S., Toetter, B., Adler, J., Tschapek, A., Doerner, J.F., Kurtenbach, S., Hatt, H., Meyer, H., Warscheid, B., and Neuhaus, E.M. (2010). Tmem16b is specifically expressed in the cilia of olfactory sensory neurons. Chem. Senses *35*, 239–245.

Reyes, J.P., López-Rodríguez, A., Espino-Saldaña, A.E., Huanosta-Gutiérrez, A., Miledi, R., and Martínez-Torres, A. (2014). Anion permeation in calcium-activated chloride channels formed by TMEM16A from Xenopus tropicalis. Pflüg. Arch. Eur. J. Physiol. *466*, 1769–1777.

Rohacs, T. (2014). Phosphoinositide regulation of TRP channels. Handb. Exp. Pharmacol. *223*, 1143–1176.

Ruiz, C., Martins, J.R., Rudin, F., Schneider, S., Dietsche, T., Fischer, C.A., Tornillo, L., Terracciano, L.M., Schreiber, R., Bubendorf, L., et al. (2012). Enhanced expression of ANO1 in head and neck squamous cell carcinoma causes cell migration and correlates with poor prognosis. PloS One *7*, e43265.

Rysavy, N.M., Shimoda, L.M.N., Dixon, A.M., Speck, M., Stokes, A.J., Turner, H., and Umemoto, E.Y. (2014). Beyond apoptosis: the mechanism and function of phosphatidylserine asymmetry in the membrane of activating mast cells. Bioarchitecture *4*, 127–137.

Sagheddu, C., Boccaccio, A., Dibattista, M., Montani, G., Tirindelli, R., and Menini, A. (2010). Calcium concentration jumps reveal dynamic ion selectivity of calcium-activated chloride currents in mouse olfactory sensory neurons and TMEM16b-transfected HEK 293T cells. J. Physiol. *588*, 4189–4204.

Sauter, D.R.P., Novak, I., Pedersen, S.F., Larsen, E.H., and Hoffmann, E.K. (2015). ANO1 (TMEM16A) in pancreatic ductal adenocarcinoma (PDAC). Pflugers Arch. *467*, 1495–1508.

Schreiber, R., Uliyakina, I., Kongsuphol, P., Warth, R., Mirza, M., Martins, J.R., and Kunzelmann, K. (2010). Expression and function of epithelial anoctamins. J. Biol. Chem. *285*, 7838–7845.

Schroeder, B.C., Cheng, T., Jan, Y.N., and Jan, L.Y. (2008). Expression cloning of TMEM16A as a calcium-activated chloride channel subunit. Cell *134*, 1019–1029.

Scudieri, P., Caci, E., Venturini, A., Sondo, E., Pianigiani, G., Marchetti, C., Ravazzolo, R., Pagani, F., and Galietta, L.J.V. (2015). Ion channel and lipid scramblase activity associated with expression of TMEM16F/ANO6 isoforms. J. Physiol. *593*, 3829–3848.

Shimizu, T., Iehara, T., Sato, K., Fujii, T., Sakai, H., and Okada, Y. (2013). TMEM16F is a component of a Ca2+-activated Cl- channel but not a volume-sensitive outwardly rectifying Cl- channel. Am. J. Physiol. Cell Physiol. *304*, C748-759.

Stephan, A.B., Shum, E.Y., Hirsh, S., Cygnar, K.D., Reisert, J., and Zhao, H. (2009). ANO2 is the cilial calcium-activated chloride channel that may mediate olfactory amplification. Proc. Natl. Acad. Sci. U. S. A. *106*, 11776–11781.

Stöhr, H., Heisig, J.B., Benz, P.M., Schöberl, S., Milenkovic, V.M., Strauss, O., Aartsen, W.M., Wijnholds, J., Weber, B.H.F., and Schulz, H.L. (2009). TMEM16B, a novel protein with calcium-dependent chloride channel activity, associates with a presynaptic protein complex in photoreceptor terminals. J. Neurosci. Off. J. Soc. Neurosci. *29*, 6809–6818.

Sui, Y., Sun, M., Wu, F., Yang, L., Di, W., Zhang, G., Zhong, L., Ma, Z., Zheng, J., Fang, X., et al. (2014). Inhibition of TMEM16A expression suppresses growth and invasion in human colorectal cancer cells. PloS One *9*, e115443.

Sun, H., Xia, Y., Paudel, O., Yang, X.-R., and Sham, J.S.K. (2012). Chronic hypoxia-induced upregulation of Ca2+-activated Cl- channel in pulmonary arterial myocytes: a mechanism contributing to enhanced vasoreactivity. J. Physiol. *590*, 3507–3521.

Suzuki, J., Umeda, M., Sims, P.J., and Nagata, S. (2010). Calcium-dependent phospholipid scrambling by TMEM16F. Nature *468*, 834–838.

Suzuki, J., Fujii, T., Imao, T., Ishihara, K., Kuba, H., and Nagata, S. (2013). Calcium-dependent phospholipid scramblase activity of TMEM16 protein family members. J. Biol. Chem. *288*, 13305–13316.

Szteyn, K., Schmid, E., Nurbaeva, M.K., Yang, W., Münzer, P., Kunzelmann, K., Lang, F., and Shumilina, E. (2012). Expression and functional significance of the Ca(2+)-activated Cl(-) channel ANO6 in dendritic cells. Cell. Physiol. Biochem. Int. J. Exp. Cell. Physiol. Biochem. Pharmacol. *30*, 1319–1332.

Taylor, K.C., and Sanders, C.R. (2017). Regulation of KCNQ/Kv7 family voltage-gated K+ channels by lipids. Biochim. Biophys. Acta Biomembr. *1859*, 586–597.

Terashima, H., Picollo, A., and Accardi, A. (2013). Purified TMEM16A is sufficient to form Ca2+-activated Cl- channels. Proc. Natl. Acad. Sci. U. S. A. *110*, 19354–19359.

Thomas-Gatewood, C., Neeb, Z.P., Bulley, S., Adebiyi, A., Bannister, J.P., Leo, M.D., and Jaggar, J.H. (2011). TMEM16A channels generate Ca^{2+}-activated Cl^- currents in cerebral artery smooth muscle cells. Am. J. Physiol. Heart Circ. Physiol. *301*, H1819-1827.

Tian, Y., Kongsuphol, P., Hug, M., Ousingsawat, J., Witzgall, R., Schreiber, R., and Kunzelmann, K. (2011). Calmodulin-dependent activation of the epithelial calcium-dependent chloride channel TMEM16A. FASEB J. Off. Publ. Fed. Am. Soc. Exp. Biol. *25*, 1058–1068.

Tien, J., Peters, C.J., Wong, X.M., Cheng, T., Jan, Y.N., Jan, L.Y., and Yang, H. (2014). A comprehensive search for calcium binding sites critical for TMEM16A calcium-activated chloride channel activity. ELife *3*.

Whitlock, J.M., and Hartzell, H.C. (2016). A Pore Idea: the ion conduction pathway of TMEM16/ANO proteins is composed partly of lipid. Pflugers Arch. *468*, 455–473.

Whitlock, J.M., and Hartzell, H.C. (2017). Anoctamins/TMEM16 Proteins: Chloride Channels Flirting with Lipids and Extracellular Vesicles. Annu Rev Physiol. *79*, 119–143.

Wu, H., Guan, S., Sun, M., Yu, Z., Zhao, L., He, M., Zhao, H., Yao, W., Wang, E., Jin, F., et al. (2015). Ano1/TMEM16A Overexpression Is Associated with Good Prognosis in PR-Positive or HER2-Negative Breast Cancer Patients following Tamoxifen Treatment. PloS One *10*, e0126128.

Xiao, Q., Yu, K., Perez-Cornejo, P., Cui, Y., Arreola, J., and Hartzell, H.C. (2011). Voltage- and calcium-dependent gating of TMEM16A/Ano1 chloride channels are physically coupled by the first intracellular loop. Proc. Natl. Acad. Sci. U. S. A. *108*, 8891–8896.

Yang, T., and Colecraft, H.M. (2016). Calmodulin regulation of TMEM16A and 16B Ca(2+)-activated chloride channels. Channels Austin Tex *10*, 38–44.

Yang, H., Kim, A., David, T., Palmer, D., Jin, T., Tien, J., Huang, F., Cheng, T., Coughlin, S.R., Jan, Y.N., et al. (2012). TMEM16F forms a Ca2+-activated cation channel required for lipid scrambling in platelets during blood coagulation. Cell *151*, 111–122.

Yang, Y.D., Cho, H., Koo, J.Y., Tak, M.H., Cho, Y., Shim, W.-S., Park, S.P., Lee, J., Lee, B., Kim, B.-M., et al. (2008). TMEM16A confers receptor-activated calcium-dependent chloride conductance. Nature *455*, 1210–1215.

Ye, W., Han, T.W., Nassar, L.M., Zubia, M., Jan, Y.N., and Jan, L.Y. (2018). Phosphatidylinositol-(4, 5)-bisphosphate regulates calcium gating of small-conductance cation channel TMEM16F. Proc. Natl. Acad. Sci. U. S. A. *115*, E1667–E1674.

Yu, K., Duran, C., Qu, Z., Cui, Y.-Y., and Hartzell, H.C. (2012). Explaining calcium-dependent gating of anoctamin-1 chloride channels requires a revised topology. Circ. Res. *110*, 990–999.

Yu, K., Zhu, J., Qu, Z., Cui, Y.-Y., and Hartzell, H.C. (2014). Activation of the Ano1 (TMEM16A) chloride channel by calcium is not mediated by calmodulin. J. Gen. Physiol. *143*, 253–267.

Yu, K., Whitlock, J.M., Lee, K., Ortlund, E.A., Cui, Y.Y., and Hartzell, H.C. (2015). Identification of a lipid scrambling domain in ANO6/TMEM16F. ELife *4*, e06901.

Zhang, Y., Zhang, Z., Xiao, S., Tien, J., Le, S., Le, T., Jan, L.Y., and Yang, H. (2017). Inferior Olivary TMEM16B Mediates Cerebellar Motor Learning. Neuron *95*, 1103-1111.e4.